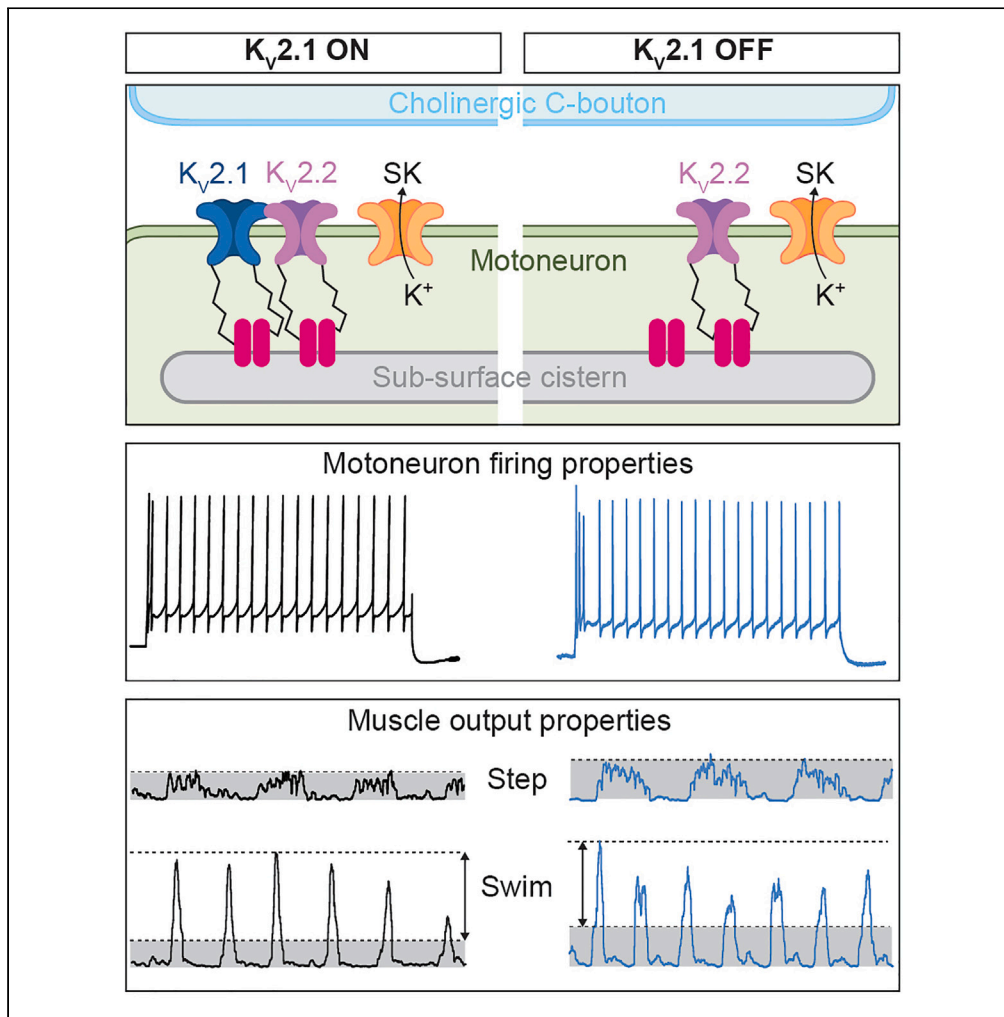


Article

# Kv2 channels do not function as canonical delayed rectifiers in spinal motoneurons



Calvin C. Smith,  
Filipe Nascimento,  
M. Görkem Özyurt,  
Marco Beato,  
Robert M.  
Brownstone

calvin.smith@ucl.ac.uk (C.C.S.)  
r.brownstone@ucl.ac.uk  
(R.M.B.)

**Highlights**

Kv2 channels do not regulate firing characteristics in mature motoneurons

Firing and muscarinic amplification are preserved in ChAT-Kv2.1 knockout mice

Behavior and motor amplification are preserved in ChAT-Kv2.1 knockout mice

With Kv2.2, motoneuron Kv2.1 channels likely play primarily structural roles

Smith et al., iScience 27, 110444  
August 16, 2024 © 2024 The Author(s). Published by Elsevier Inc.  
<https://doi.org/10.1016/j.isci.2024.110444>



## Article

## Kv2 channels do not function as canonical delayed rectifiers in spinal motoneurons

Calvin C. Smith,<sup>1,\*</sup> Filipe Nascimento,<sup>1</sup> M. Görkem Özyurt,<sup>1</sup> Marco Beato,<sup>2</sup> and Robert M. Brownstone<sup>1,3,\*</sup>

## SUMMARY

The increased muscular force output required for some behaviors is achieved via amplification of motoneuron output via cholinergic C-bouton synapses. Work in neonatal mouse motoneurons suggested that modulation of currents mediated by post-synaptically clustered  $K_V2.1$  channels is crucial to C-bouton amplification. By focusing on more mature motoneurons, we show that conditional knockout of  $K_V2.1$  channels minimally affects either excitability or response to exogenously applied muscarine. Similarly, unlike in neonatal motoneurons or cortical pyramidal neurons, pharmacological blockade of  $K_V2$  currents has minimal effect on mature motoneuron firing *in vitro*. Furthermore, *in vivo* amplification of electromyography activity and high-force task performance was unchanged following  $K_V2.1$  knockout. Finally, we show that  $K_V2.2$  is also expressed by spinal motoneurons, colocalizing with  $K_V2.1$  opposite C-boutons. We suggest that the primary function of  $K_V2$  proteins in motoneurons is non-conducting and that  $K_V2.2$  can function in this role in the absence of  $K_V2.1$ .

## INTRODUCTION

Animals can produce a vast repertoire of behaviors by altering spatiotemporal patterns of muscle contractions, which are governed by the motoneurons that innervate them. Therefore, motoneuron activity must be regulated so as to support diverse motor outputs. In addition to muscle fiber type properties, the strength of muscle contraction is governed by the number of active innervating motoneurons and their firing frequencies.<sup>1</sup> Thus, to understand the neural mechanisms of behavior, it is essential to understand how motoneurons produce repetitive spike trains.

The relationship between the inputs a motoneuron receives and its outputs is often represented by a “frequency-current” or *f-I* curve, with the current being that injected through a recording electrode. Motoneuronal excitability, represented by the slope(s) of the linear segment(s) (gain) of this curve, can be altered in a task-dependent manner by neuromodulator systems. One system that can increase the gain is that comprised of presynaptic C-boutons, named because of their association with specialized endoplasmic reticulum (ER) called “subsurface cisterns”.<sup>2</sup> These boutons arise from cholinergic V0c interneurons.<sup>3,4</sup> The postsynaptic motoneuron membrane apposing C-boutons includes clusters of many proteins, including type 2 muscarinic acetylcholine (M2) receptors,<sup>5</sup> slow calcium-dependent potassium channels (SK2, SK3)<sup>6</sup> and voltage-gated delayed rectifier potassium channels ( $K_V2.1$ ).<sup>7</sup> These synapses mature over the first three weeks of post-natal development in mice in parallel with the development of weight-bearing locomotor function.<sup>8</sup> And in the adult mouse, this system is recruited for high force outputs such as the extensor stroke in swimming.<sup>4</sup> But how activation of M2 receptors leads to the increase in excitability needed for these tasks remains elusive, leaving a significant hole in our understanding of movement.

It has been hypothesized that M2 receptor activation affects  $K_V2.1$  function to actuate C-bouton-mediated amplification.<sup>7,9,10</sup>  $K_V2$  channels are widely expressed through the central nervous system.<sup>11</sup> There are two main  $K_V2$  subunits, *Kcnc1* ( $K_V2.1$ ) and *Kcnc2* ( $K_V2.2$ ), which share similar biophysical properties, and are often, but not always, co-expressed.<sup>12–15</sup> The canonical function of  $K_V2$  channels is to regulate neuronal excitability through delayed rectifier  $K^+$  currents.<sup>16</sup> Their importance in neuronal function is evident by clinical reports of people with *Kcnc1* mutations, who have a myriad of problems including reduced cognitive capacity and epilepsy.<sup>17,18</sup> About one-half of the 26 reported people are hypotonic, with 2/3 of these people having signs in early life. But mice with *Kcnc1* deletions are hyperactive; their problems are not in motoneuron function *per se*, and they are not hypotonic.<sup>19</sup> These results do not support the hypothesis that  $K_V2.1$  channels are required for motor output. And they do not shed light on what the role of these channels in motoneurons might be.

Using  $K_V2$  ( $K_V2.1$  and  $K_V2.2$ ) channel blockers, several groups have suggested significant roles for  $K_V2.1$  conductances in C-bouton-mediated amplification in neonatal rodent motoneurons.<sup>20–22</sup> Although results were not all entirely consistent between the studies, overall they suggested that when active, C-boutons recruit local  $K_V2.1$  channels to maintain narrow spikes and fast afterhyperpolarization (fAHP) amplitudes, thus supporting high-frequency firing by preventing  $Na^+$  channel inactivation and the resultant depolarization block. That is, current work suggests  $K_V2.1$  channels have significant conducting roles.

<sup>1</sup>Department of Neuromuscular Diseases, UCL Queen Square Institute of Neurology, University College London, London WC1N 3BG, UK

<sup>2</sup>Department of Neuroscience, Physiology, and Pharmacology, University College London, London WC1E 6BT, UK

<sup>3</sup>Lead contact

\*Correspondence: calvin.smith@ucl.ac.uk (C.C.S.), r.brownstone@ucl.ac.uk (R.M.B.)

<https://doi.org/10.1016/j.isci.2024.110444>



In motoneurons,  $K_v2.1$  channels at C-bouton synapses are densely clustered. In other neurons, this clustering results from a proximal restriction and clustering (PRC) domain, which was added to the C-terminal tail of  $K_v2$  during evolution.<sup>16,23</sup> Although  $K_v2$  channels in this configuration are non-conducting,<sup>24,25</sup> spatial aggregation of  $K_v2$  via the PRC domain does not regulate conductance *per se*, because PRC mutations that cause de-clustering do not increase  $K_v2$  conductance.<sup>26,27</sup> The  $K_v2$  PRC domain confers a structural role by binding to VAPs (vesicle associated membrane protein (VAMP) associated proteins) located on the endoplasmic reticulum (ER) membrane (EM), physically linking the plasma membrane (PM) to within 10 nm.<sup>28–30</sup> Recent work has revealed that the tight ER-PM junctions (EPJs) conferred by  $K_v2$  are essential for the spatial and functional coupling of several local  $Ca^{2+}$  signaling mechanisms crucial to cellular physiology.<sup>27,31,32</sup> For example, in hippocampal neurons,  $K_v2.1$  promotes spatial and functional coupling of L-type calcium channels and ryanodine receptors (RyR) to mediate local calcium sparks.<sup>33</sup> Although RyR have not been identified in motoneurons, given the calcium dependence of proteins clustered at C-boutons and the recent discovery of VAP expression in C-bouton post-synaptic domains,<sup>9</sup> it is plausible that these dense clusters of  $K_v2.1$  proteins could serve similar non-conducting roles in motoneurons.

Taken together, the role of these prominent  $K_v2.1$  channels in regulating motoneuron firing and in C-bouton modulation remains unclear. We therefore aimed to define  $K_v2.1$  function in mature motoneurons from electrophysiology through to animal behavior. We made a conditional knock-out (cKO) mouse in which cholinergic neurons (including motoneurons) lacked  $K_v2.1$  channels. We then used whole-cell patch clamp electrophysiology to compare the firing characteristics of mature  $K_v2.1^{ON}$  (control) and ChAT- $K_v2.1^{OFF}$  motoneurons and the effects of the specific  $K_v2$  channel blocker guangxitoxin-1E (GxTX-1E) on these properties. We repeated these experiments in early post-natal control motoneurons to assess whether developmental clustering of  $K_v2.1$  channels influences their role in regulating firing. To determine the role of  $K_v2.1$  in C-bouton function, we activated M2 receptors *in vitro* using muscarine and compared excitability changes in control and  $K_v2.1$  cKO motoneurons. Finally, to assess whether  $K_v2.1$  influences motor amplification, we studied high-force output behaviors while recording electromyography (EMG) activity in hindlimb muscles. In summary, we found that  $K_v2.1$  does not regulate mature motoneuron physiology or behavior, and suggest that  $K_v2$  channels primarily play a non-conducting role. Furthermore, we show that motoneurons also express  $K_v2.2$ , suggesting it can subsume the non-conducting roles of  $K_v2$  channels to maintain C-bouton function.

## RESULTS

### cKO of $K_v2.1$ does not alter motoneuron passive membrane properties

In order to investigate the contribution of  $K_v2.1$  channels to motoneuron physiology, we aimed to eliminate  $K_v2.1$  from motoneurons through multi-generational crossing of ChAT-IRES-Cre (ChAT<sup>(Cre/Cre)</sup>) mice with homozygous floxed *Kcnb1* mice (*Kcnb1*<sup>(f/f)</sup>) to generate ChAT<sup>(Cre/wt);Kcnb1</sup>(<sup>-/-</sup>), called here ChAT- $K_v2.1^{OFF}$  mice (Figure 1A). To validate this strategy's efficacy, we proceeded with immunohistochemical labeling using antibodies against ChAT and  $K_v2.1$  in ChAT- $K_v2.1^{OFF}$  and littermate controls (ChAT<sup>(w/w);Kcnb1</sup>(<sup>f/f</sup>) or  $K_v2.1^{ON}$  mice, Figures 1B–1E2). Our analyses showed similar  $K_v2.1$  punctae density in the dorsal horn of both genotypes (Figure 1F) but large reductions in the intermediate (Figure 1G) and ventral horns (Figure 1H), indicating the strategy was successful, given that cholinergic neurons, including motoneurons are found most densely in these regions. We found no  $K_v2.1$  labeling on motoneuron somata of ChAT- $K_v2.1^{OFF}$  mice, suggesting that any residual punctae in the ventral horns were associated with non-cholinergic neurons (Figures 1D–1E2).

Having confirmed that ChAT- $K_v2.1^{OFF}$  motoneurons are devoid of  $K_v2.1$ , we next performed whole-cell current clamp experiments to define whether the electrical properties of mature (P13–21)  $\alpha$ -motoneurons were affected by channel absence. We first assessed the passive membrane properties of large control and ChAT- $K_v2.1^{OFF}$  motoneurons under resting conditions (no C-bouton activation) and found a small mean difference in resting membrane potential, but input resistance, whole-cell capacitance, time constant, and rheobase were all similar (Figure 1I–1M).

### Motoneuron firing and action potential characteristics are similar in control and ChAT- $K_v2.1^{OFF}$ mice

$K_v2.1$  delayed rectifier currents are important for maintaining spike shape in many neurons, with numerous studies showing that their block increases spike width and reduces amplitude of both the fast AHP (fAHP) and the spike itself.<sup>20,34,35</sup> However, we found that ChAT- $K_v2.1^{OFF}$  and control motoneurons had similar spike amplitudes (Figures 2A and 2B), AP ½ widths (Figure 2C), and fAHP amplitudes (Figure 2D).

Although small conductance calcium activated potassium (SK) currents are the main conductances contributing to the medium AHP (mAHP),  $K_v2.1$  delayed rectifier currents have recently been suggested as an auxiliary mAHP conductance in motoneurons.<sup>22</sup> Our analyses showed no consistent difference in mAHP amplitudes (Figure 2E) or ½ decay (Figure 2F).

Unlike single evoked spikes, action potentials during repetitive firing are subject to conductances that have longer time constants,<sup>36</sup> and therefore their morphology may be differentially affected.<sup>21</sup> Thus, we also assessed mean AP characteristics at 3 times the threshold for repetitive firing, and found that spike amplitude (mean AP amplitude-3T, Figure 2G), AP ½ width (mean AP ½ width-3T, Figure 2H), and inter spike trough (mean trough amplitude-3T, Figure 2I) were similar in control and ChAT- $K_v2.1^{OFF}$  motoneurons.

Next, we compared repetitive firing properties of motoneurons from both groups. The maximum instantaneous frequency of repetitive firing during the entire 500 ms pulse (max overall frequency, Figures 2J–2L) was higher in ChAT- $K_v2.1^{OFF}$  motoneurons compared to control, however, the slope of the *f*-*I* curve was similar between groups (max overall frequency slope, Figure 2M). In addition, the maximum instantaneous frequencies of first two spikes (max 1<sup>st</sup> interval frequency, Figure 2N), and *f*-*I* slopes of this interval (1<sup>st</sup> interval slope Figure 2O) of control and ChAT- $K_v2.1^{OFF}$  motoneurons were similar. Taken together, these results suggest that while there is no difference in excitability of the two populations of motoneurons,  $K_v2.1$  conductances may limit maximum sustained firing rates.

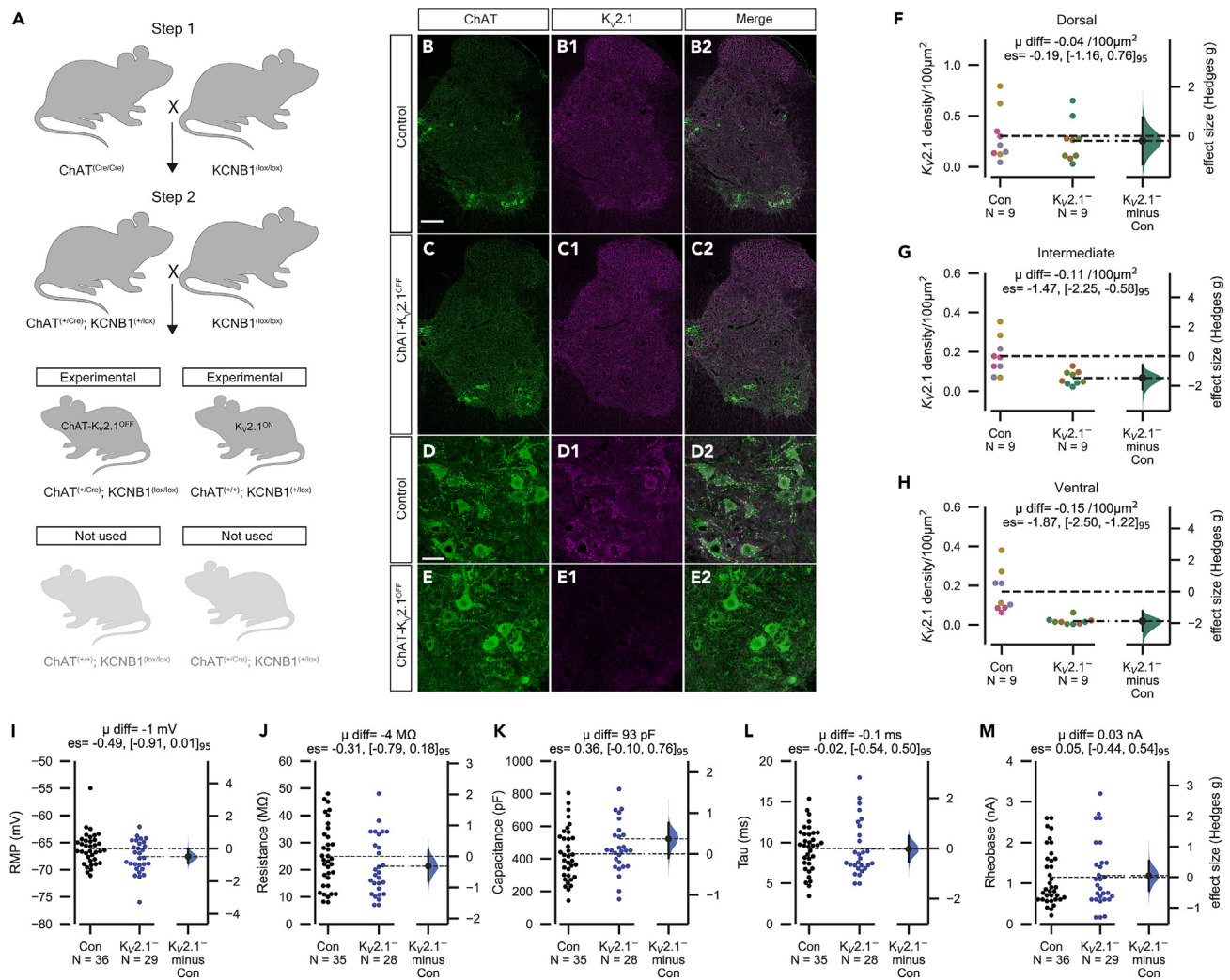


**Figure 1. cKO of Kv<sub>v</sub>2.1 does not alter motoneuron passive membrane properties**

(A) Two main breeding steps were used to generate experimental animals. In step 1 (first cross), homozygous ChAT<sup>(cre/cre)</sup> mice were crossed with KCNB1<sup>(lox/lox)</sup> mice to produce heterozygous ChAT<sup>(+/cre); KCNB1<sup>(+/lox)</sup> offspring. For step 2, ChAT<sup>(+/cre); KCNB1<sup>(+/lox)</sup> mice were bred with KCNB1<sup>(lox/lox)</sup> mice to produce experimental (blue) ChAT<sup>(+/cre); KCNB1<sup>(lox/lox)</sup> mice and control mice (gray).</sup></sup></sup>

(B–C2) Confocal photomicrographs (20× tile scans, 1 μm optical section) of spinal cord hemisections from a control (A–C) and ChAT-Kv<sub>v</sub>2.1<sup>OFF</sup> mouse showing ChAT and Kv<sub>v</sub>2.1 labeling.

(D–D2) 20× z stack images from motor pool of a control mouse spinal cord.

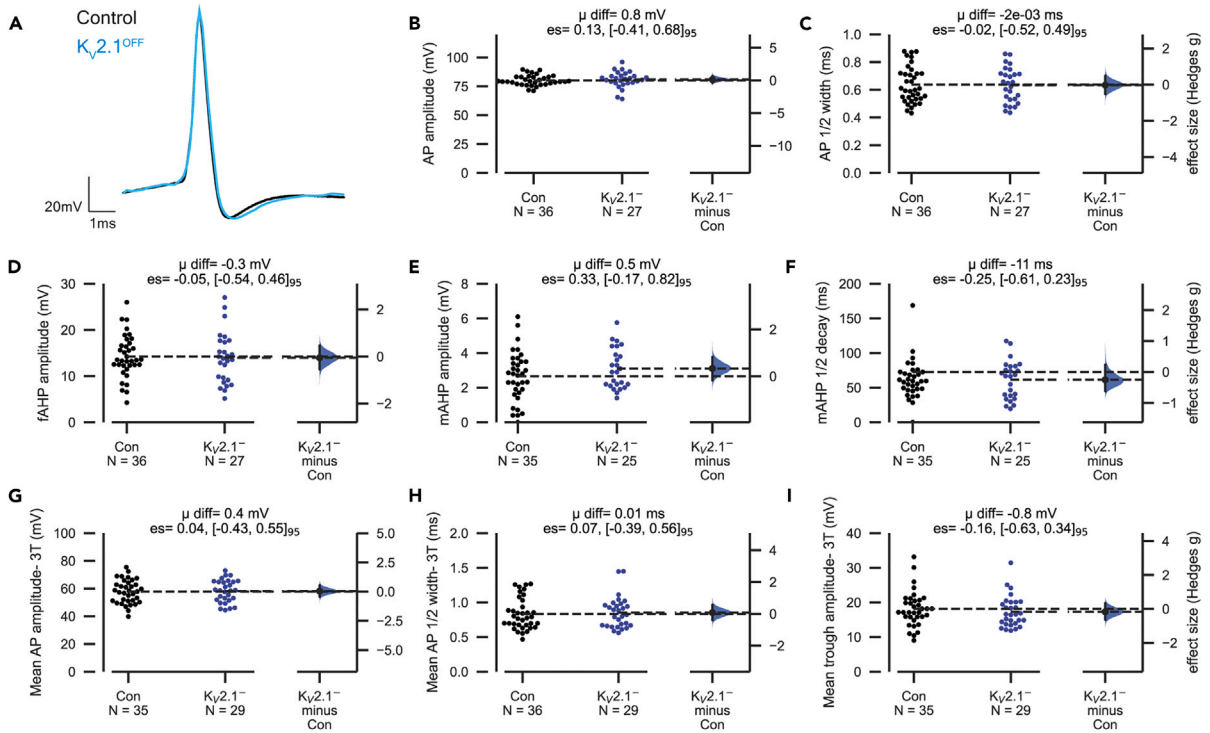
(E–E2) As in D–D2, but from a ChAT-Kv<sub>v</sub>2.1<sup>OFF</sup> mouse. Note the absence of Kv<sub>v</sub>2.1<sup>+</sup> puncta on motoneurons following conditional knockout.

(F–H) Gardner-Altman estimation plots showing Kv<sub>v</sub>2.1 density in dorsal (F), intermediate (G) and ventral (H) regions. Density was calculated by counting the number of Kv<sub>v</sub>2.1 punctae within a region of interest (ROI). The dimensions of the ROI were the same for each section. Each point represents one section, with different fill colors representing sections from different animals. Scale bar, 100 μm in B–C2 and 40 μm in D–E2. Three random, free floating slices (30 μm thickness) were quantified per animal (Control, N = 9 slices from 3 animals; ChAT-Kv<sub>v</sub>2.1<sup>OFF</sup>, N = 9 slices from 3 animals, all females).

(I–M) Gardner-Altman plots comparing resting membrane potential (RMP, I), input resistance (J), whole cell capacitance (K), time constant (tau, L), and rheobase (M) between control and ChAT-Kv<sub>v</sub>2.1<sup>OFF</sup> mice. Experimental unit (N) = motoneurons recorded from 23 control (n = 9 females, 14 males) and 14 ChAT-Kv<sub>v</sub>2.1<sup>OFF</sup> mice (n = 7 females, 7 males).

In some neurons, Kv<sub>v</sub>2 delayed rectifier currents ensure Na<sup>+</sup> channel recovery by maintaining fast action potential (AP) repolarization kinetics, thereby preventing depolarizing block.<sup>34,35</sup> We therefore assessed whether cKO of Kv<sub>v</sub>2.1 affected the current threshold at which membrane depolarization blocked spike production (Figure 2P). Despite a lack of Kv<sub>v</sub>2.1, ChAT-Kv<sub>v</sub>2.1<sup>OFF</sup> motoneurons entered depolarizing block at similar current thresholds as control motoneurons, suggesting Kv<sub>v</sub>2.1 contributes little to preventing depolarizing block in spinal motoneurons.

Action potential characteristics



Firing characteristics

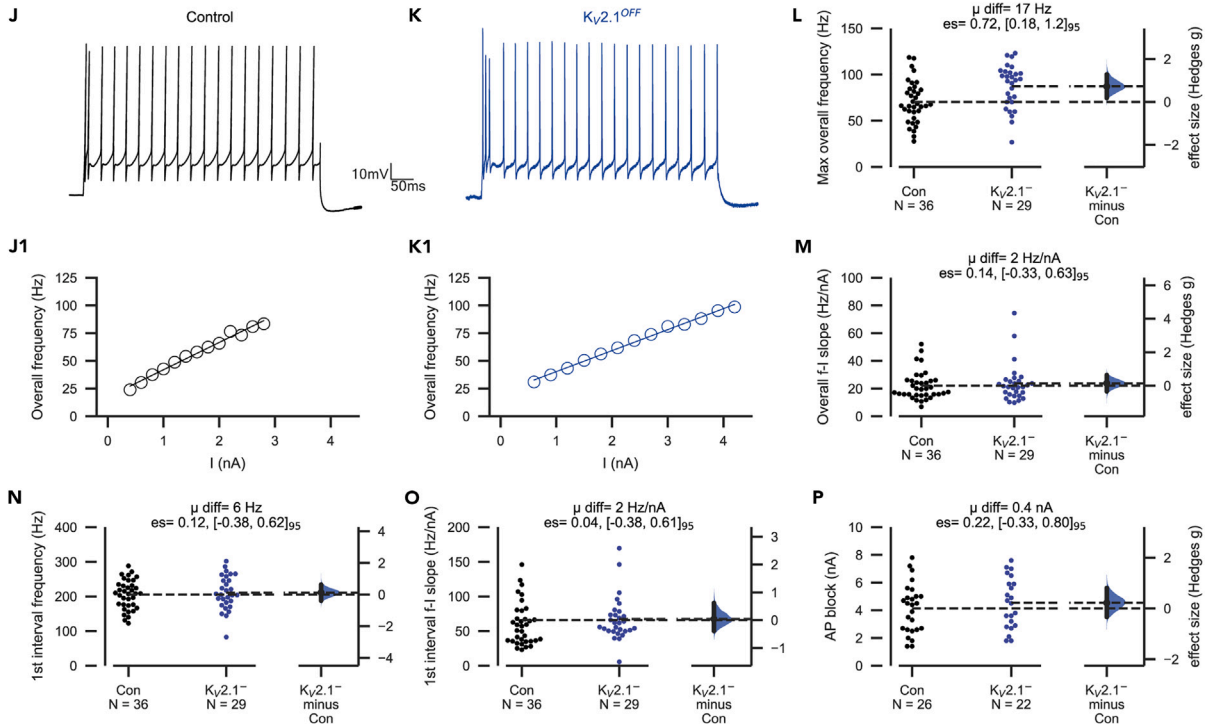


**Figure 2. Motoneuron firing and action potential characteristics are similar in control and ChAT-Kv2.1<sup>OFF</sup> mice**

Patch clamp electrophysiology was used to assess various firing and action potential characteristics of lumbar motoneurons in control and ChAT-Kv2.1<sup>OFF</sup> mice. (A) Representative averages of 15–30 single action potentials (AP) evoked with a 20 ms current pulse in control (Con, black) and ChAT-Kv2.1<sup>OFF</sup> (blue) motoneurons.

(B–F) Gardner-Altman estimation plots for action potential amplitude (B), ½ width (C), fast afterhyperpolarisation amplitude (fAHP, D), medium afterhyperpolarisation amplitude (mAHP, E), mAHP ½ decay time (F).

(G–I) As is H–L, but mean of all APs in a 500 ms pulse are taken at 3x threshold (3T) for repetitive firing. AP amplitude is shown in (M), mean AP ½ width-3T (N), and mean AHP-3T (O). Experimental unit (N) = motoneurons recorded from 23 control (n = 9 females, 14 males) and 14 ChAT-Kv2.1<sup>OFF</sup> mice (n = 7 females, 7 males). Mean difference is abbreviated to “μ diff”, and hedges g estimation statistic is represented by “es”.

(J and K) Representative traces from a control (Con, black) and ChAT-Kv2.1<sup>OFF</sup> motoneuron (blue) at 3x threshold for repetitive firing. (J1–K1) Representative *f*-I plots for control (black) and ChAT-Kv2.1<sup>OFF</sup> motoneurons (blue).

(L) Gardner-Altman estimation plot for maximum overall frequency, calculated as the mean instantaneous frequency between all spikes within a 500 ms train.

(M) The slope of the *f*-I curve for the overall frequency, calculated from the first linear portion of the plot, as indicated by lines fitted in J1–K1.

(N) The maximum instantaneous frequency of the first inter-spike interval in a 500 ms train.

(O) As in M, but the *f*-I curve is only calculated for the first inter-spike interval.

(P) The current threshold for depolarizing block (spike failure). Control and ChAT-Kv2.1<sup>OFF</sup> groups are plotted on the left axes and the bootstrapped sampling distribution (5000 reshuffles) for Hedges g effect sizes are plotted on the right. Each point represents a single motoneuron.

Together, comparisons of firing characteristics and AP morphology from mature (P13–21) control and ChAT-Kv2.1<sup>OFF</sup> motoneurons indicate that either Kv2.1 channels have minimal role in regulating firing capabilities or that there were effective compensatory mechanisms following their loss.

**Kv2 block by GxTX-1E has minimal effect on motoneuron firing or action potential characteristics**

Given that various mechanisms could mask associated deficits in ChAT-Kv2.1<sup>OFF</sup> motoneurons, we next assessed the role of Kv2.1 channels in shaping motoneuron firing characteristics pharmacologically. We used the Chinese tarantula toxin guangxitoxin-1E (GxTX-1E), which at 100 nM potently and selectively inhibits Kv2 channels.<sup>20,22,34,37,38</sup> Because Kv2.1 channels have recently been suggested to play a significant role in regulating motoneuron firing, we hypothesized GxTX-1E would significantly alter firing characteristics in control but not ChAT-Kv2.1<sup>OFF</sup> motoneurons.

To confirm that in our hands GxTX-1E does not have significant effects on passive membrane properties of wild-type motoneurons,<sup>20,22</sup> we first measured these effects in both our control and ChAT-Kv2.1<sup>OFF</sup> motoneurons by measuring voltage responses to sub-threshold and threshold current steps (Figures S1A–S1E). In line with previous work, there were no effects of the toxin on resting membrane potential in either condition (Figure S1B). Similarly, we found no consistent effect of GxTX-1E on input resistance (Figure S1C) or whole-cell capacitance (Figure S1D) in either control or ChAT-Kv2.1<sup>OFF</sup> motoneurons. In contrast, we saw small increases in the rheobase of both ChAT-Kv2.1<sup>OFF</sup> and control motoneurons (Figure S1E), suggesting that GxTX-1E had effects on conductances other than Kv2.1.

We next measured the effects of GxTX-1E on action potential morphology. We found no significant effects on AP amplitude (Figures 3A and 3B), AP half-width (Figure 3C), or fAHP amplitude (Figure 3D). Recent evidence suggested that Kv2.1 conductances contribute to the mAHP.<sup>22</sup> In agreement, we found that GxTX-1E had a medium effect (Hedge’s *g* = 0.6) on mAHP amplitudes in ChAT-Kv2.1<sup>OFF</sup> motoneurons, and a small effect (Hedge’s *g* = 0.3) in control motoneurons (Figure 3E). There were no effects of the toxin on mAHP half decay (Figure 3F). Because GxTX-1E-mediated decreases in mAHP amplitude were seen in both control and ChAT-Kv2.1<sup>OFF</sup> motoneurons, it is likely that GxTX-1E acted on conductances other than Kv2.1.

GxTX-1E block of Kv2 channels also had little effect on motoneuron repetitive firing properties. The slopes of the *f*-I relationship for overall and initial frequency were unaltered by GxTX-1E in both ChAT-Kv2.1<sup>OFF</sup> (Figures 3G–3I) and control motoneurons. Similarly, we found little effect of GxTX-1E on the maximum overall firing frequency for either ChAT-Kv2.1<sup>OFF</sup> or control motoneurons (Figure 3J). However, GxTX-1E did lead to small reductions in the maximum first interval firing frequency in both ChAT-Kv2.1<sup>OFF</sup> and control motoneurons (Figure 3K), again suggesting that the toxin was acting on conductances other than Kv2.1.

In cells in which Kv2.1 has a significant conducting role, GxTX-1E reduces the threshold for depolarizing block of action potentials.<sup>34,35,39</sup> However, GxTX-1E had no effect on the threshold for AP block in either ChAT-Kv2.1<sup>OFF</sup> or control motoneurons (Figure 3L).

In summary, apart from small increases in rheobase and decreases in frequency of the first interspike interval and mAHP amplitude in both ChAT-Kv2.1<sup>OFF</sup> and control motoneurons, GxTX-1E had little effect on firing capabilities or AP characteristics. Importantly, GxTX-1E effects were seen in both genotypes, suggesting that the toxin was acting on conductances other than Kv2.1 (possibly Kv2.2, see in the following text).

**Kv2 block increases excitability of cortex layer V pyramidal neurons**

The results to this point suggest that under resting conditions (no C-bouton activation), Kv2.1 does not play a significant role in regulating motoneuron firing in motor mature (P13–21) mice. Because these results were not consistent with studies in younger animals,<sup>20–22</sup> we next proceeded with a positive control by testing our protocol on layer V cortical pyramidal neurons, in which Kv2.1 channels have significant electrophysiological functions.<sup>38–40</sup>

We found that GxTX-1E caused significant changes to individual pyramidal neuron action potential characteristics with large effect sizes in pyramidal neurons (Figure S2). As demonstrated in similar studies assessing the effect of inhibiting Kv2.1 in cortical and other brain

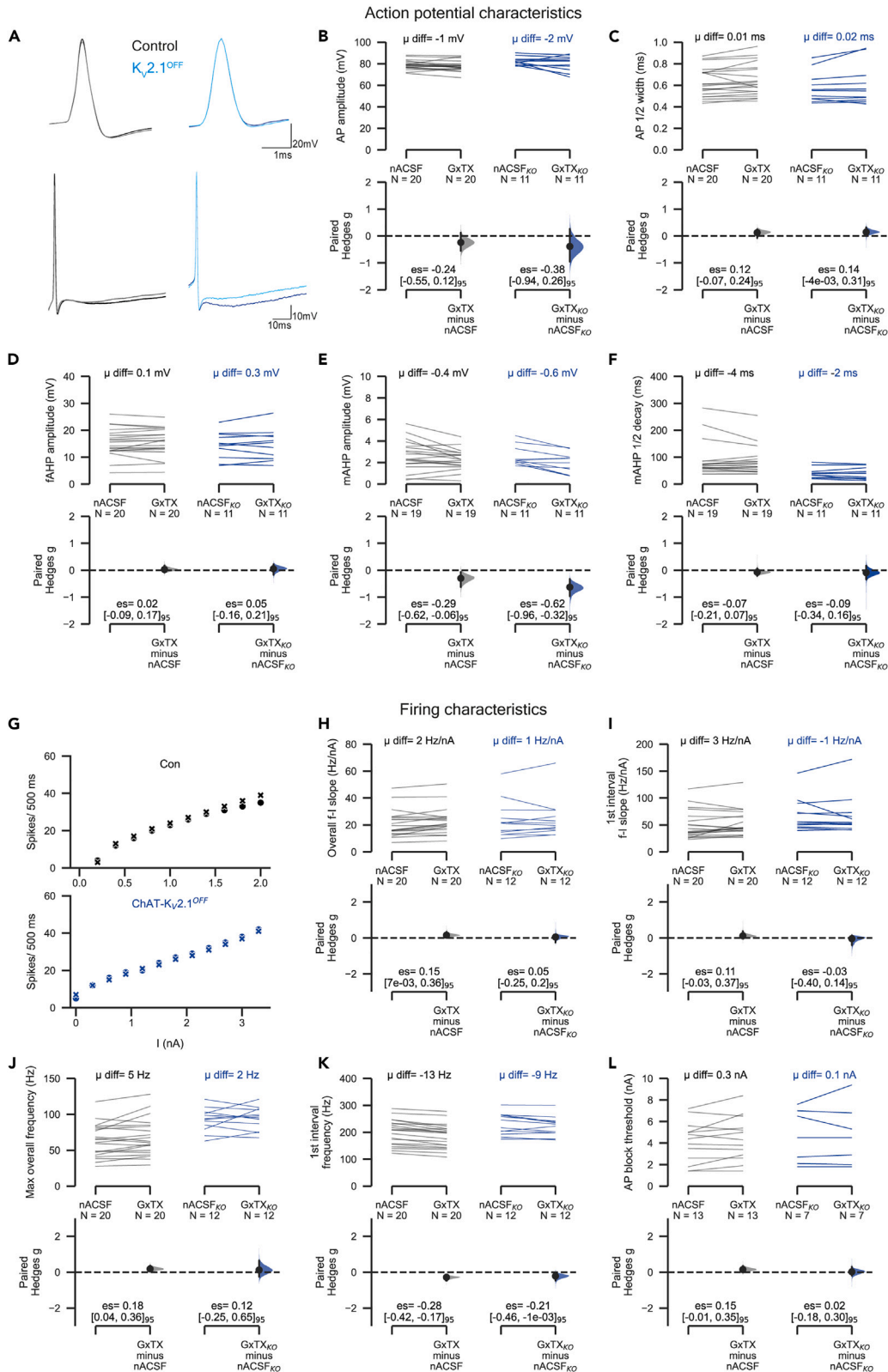


**Figure 3. K<sub>v</sub>2 block by GxTX-1E has minimal effect on motoneuron maximal firing or action potential characteristics**

See also Figures S1–S3.

(A–F) Comparing the effects of K<sub>v</sub>2 inhibition with GxTX-1E on action potential characteristics. (A) The upper panel shows representative single evoked AP traces from control (left) and ChAT-K<sub>v</sub>2.1<sup>OFF</sup> motoneurons (right). The dark colors (black, blue) show spike morphology in the presence of nACSF only and the light colors (gray, sky blue) show morphology after 10 min perfusion with 100 nM GxTX-1E. The lower panels show longer sweeps in order to visualize the mAHP. (B–F) Paired Hedges *g* for control (left) and ChAT-K<sub>v</sub>2.1<sup>OFF</sup> (right) motoneurons: (B) shows the spike amplitude, (C) is action potential ½ width, (D) the fAHP amplitude, (E) is the mAHP amplitude, and (F) is the mAHP ½ decay time. (G) Scatterplots of spike number in response to increasing current input for representative motoneurons from control (upper graph, black) and ChAT-K<sub>v</sub>2.1<sup>OFF</sup> mice (lower graph, blue). Spike number in motoneurons perfused with nACSF only is plotted using “O” and following 10 min GxTX-1E is plotted with “X”. (H–L) Paired Hedges *g* for overall *f*-I slope (H), 1<sup>st</sup> interval *f*-I slope (I), maximum overall frequency (J), maximum 1<sup>st</sup> interval frequency (K), and AP block threshold (L) in control (left) and ChAT-K<sub>v</sub>2.1<sup>OFF</sup> (right) motoneurons are shown in Cumming paired estimation plots with Hedges *g* distributions shown in the following text. Number of animals used was as follows: control = 13 (6 females, 7 males), ChAT-K<sub>v</sub>2.1<sup>OFF</sup> = 6 (4 females, 2 males). Experimental unit (*N*) = motoneurons. Mean difference is abbreviated to “μ diff”, and hedges *g* estimation statistic is represented by “es”. See also Figures S1 and S2.

neurons,<sup>35,38–41</sup> we found large increases in AP ½-width (Figure S2C), as well as decreases in spike amplitude (Figures S2A and S2B) and fAHP (Figure S2D). GxTX-1E also caused a small decrease in mAHP amplitude (Figure S2E), but mAHP ½-decay was not affected (Figure S2F).

GxTX-1E also had effects on repetitive firing of cortical neurons, leading to increases in overall *f*-I slope (Figures S2G–S2I) and initial interval *f*-I slope (Figure S2J). There was no consistent effect on maximum firing frequencies: both the overall (Figure S2K) and initial (Figure S2L) maximum frequencies were similar in both conditions. This resulted from the neurons reaching depolarizing block at significantly lower current thresholds (Figure S2M).

In summary, we found that GxTX-1E block of K<sub>v</sub>2 channels had little effect on the firing capacity of mature control and ChAT-K<sub>v</sub>2.1<sup>OFF</sup> motoneurons. But the same experiments in layer 5 cortical pyramidal neurons greatly increased excitability and maximum firing, in line with previous studies. The clear differences in paired sample effect sizes (Hedges *g*) on the parameters assessed suggest that, compared to pyramidal neurons, K<sub>v</sub>2 channels (both 2.1 and 2.2) play only a minor role in regulating motoneuron repetitive firing (Figure S2N).

**Post-natal clustering does not significantly alter K<sub>v</sub>2 regulation of motoneuron firing**

During post-natal motoneuron development, K<sub>v</sub>2.1 channels organize into high-density macroclusters,<sup>8</sup> a configuration associated with non-conducting channels<sup>24</sup> and that may play a role in neurodevelopment in the forebrain.<sup>42</sup> Because our patch clamp experiments were done at an age (post-natal week 3) at which K<sub>v</sub>2.1 clusters appear mature,<sup>8</sup> we investigated whether developmental clustering of channels might contribute to differences in our results compared to studies in young motoneurons.<sup>20–22</sup>

We first used immunohistochemistry to quantitatively assess the expression and membrane localization of K<sub>v</sub>2.1 channels in lumbar motoneurons from mice aged P2–P3 (neonatal, Figures 4A–4A3), P6–P7 (transition) and P21 (motor mature, Figures 4B–4B3). The density of VACHT<sup>ON</sup> C-boutons increased with development (Figure 4C), while K<sub>v</sub>2.1 density (# puncta pre 100μm<sup>2</sup>) decreased between P3 and P21 (Figure 4D). We also saw an increase in the percentage of K<sub>v</sub>2.1 localized opposite C-boutons with age (Figure 4E). These data show that in neonatal motoneurons, K<sub>v</sub>2.1 channels are mainly organized in dispersed microclusters (Figure 4F), many of which are not associated with C-boutons (Figure 4G). As post-natal development progresses and motoneurons (Smith and Brownstone, 2020) and motor behaviors mature,<sup>43</sup> large macroclusters of K<sub>v</sub>2.1 channels form opposite C-bouton synapses.

We next compared the effects of GxTX-1E on immature and mature motoneuron firing and AP characteristics. As with mature motoneurons (described previously), GxTX-1E had minimal effect on overall *f*-I slope (Figure 4H), first interval *f*-I slope (Figure 4I), maximum overall frequency (Figure 4J), or maximum first interval frequency (Figure 4K). GxTX-1E increased the AP ½-width by 0.10 ms in young motoneurons compared to 0.01 ms in mature motoneurons (Figure 4L), suggesting a contribution of K<sub>v</sub>2 conductances to action potential repolarization at this stage. As with mature motoneurons, there was no effect of GxTX-1E on fAHP amplitude in young motoneurons (Figure 4M). Together, these results show that K<sub>v</sub>2 conductances have minimal effects even in neonatal motoneuron firing but do have a significant effect on AP repolarization in neonatal motoneurons.

We next attempted to measure K<sub>v</sub>2 currents in voltage clamp experiments with sodium and calcium currents blocked. Being concerned that the large amplitudes of the potassium currents would preclude quantification because of the large voltage error induced by series resistance in the presence of high-amplitude currents, we sought, through a series of 2-electrode voltage clamp experiments, to determine whether it would be reasonable to make even a qualitative assessment (Figure S3A). When current was passed through the V-clamp electrode, while simultaneously measuring voltage with a second, voltage follower, electrode, the voltage error was indeed very high for currents above 2–3 nA (albeit the true voltage error was less than predicted, Gray and Santin, 2023). Since K currents in motoneurons can be as large as 30 nA (Figures S3B and S3C), we could not accurately measure the I-V relationship. However, we reasoned that, although quantification would be inaccurate, if we saw no change in currents with GxTX-1E, then there would be little in the way of K<sub>v</sub>2 conductance. Indeed, while there is potential evidence of a reduction in total potassium currents (“measured” as ~5%) at early post-natal stages, there was none in the 3<sup>rd</sup> post-natal week (Figure S3D). These results are consistent with the aforementioned results, showing little effect of K<sub>v</sub>2 conductances on motoneuron firing.

Taken together, even at neonatal ages when there is less clustering, K<sub>v</sub>2 channels contribute minimally to overall potassium currents, and at mature stages, their conductance does not contribute to motoneuron firing. That is, the lack of effects on motoneuron firing of both the





**Figure 4. Post-natal clustering does not significantly alter  $K_v2$  regulation of motoneuron firing**

(A and B) 3D projections of Z-stacks taken at 60x on a confocal microscope showing raw GFP expression under the Hb9 promoter (A and B), immuno-labeling of  $K_v2.1$  (A1 and B1) and VAcHT (A2 and B2, depicting presynaptic C-boutons). Images merged in (A3 and B3).

(C and D) Intensity plots (intensity/maximum intensity) showing the distribution of VAcHT and  $K_v2.1$  signal around the perimeter of a 60x confocal image (1 $\mu$ m section) of a representative motoneuron from a P3 (F) and P21 (G) mouse.

(E–G) Gardner-Altman estimation plots for the density of VAcHT<sup>+</sup> C-boutons (E), density of  $K_v2.1$  (F), and %  $K_v2.1$  clustered to C-boutons on individual motoneurons from throughout development (G). Values for individual cells are plotted (color coded by animal) on the upper axes and the hedges g effect sizes for P6-7 vs. P21 vs P6-7 on the lower axes. Note that measurements were taken at P2, 3, 6, 7 and P21, however cells were analyzed in 3 age groups. A total of 137 motoneurons were sampled from 8 animals (P2-3: 3 mice, N = 48; P6-7: 3 mice N = 51; P21: 2 mice, N = 36; all females).

(H–M) Cumming paired estimation plots showing paired Hedges g for overall frequency slope (H), 1<sup>st</sup> interval frequency slope (I), maximum overall frequency (J), maximum 1<sup>st</sup> interval frequency (K), AP 1/2 width (L), and fAHP (M) in young (P2-7, left) and motor mature (P13-21, right) motoneurons. The number of motoneurons and animals used for each age was as follows: P2-3 = 8 cells from 4 mice (2 males, 2 females); P6-7 = 10 cells from 5 mice (2 males, 3 females; 9 animals total for the <P7 group), for mature motoneurons (P13+) 13 were mice were used (6 females, 7 males). Scale bar in (A), 20 $\mu$ m. Mean difference is abbreviated to “ $\mu$  diff”, and hedges g estimation statistic is represented by “es”. See also [Figure S3](#).

developmental cKO of  $K_v2.1$  channels and acute pharmacological block of  $K_v2$  channels do not appear to be due to developmental differences such as channel clustering.

**Muscarine-induced increase in excitability is preserved in ChAT- $K_v2.1^{OFF}$  motoneurons**

Motoneuron  $K_v2.1$  channels are opposed to, and thought to be modulated by C-boutons via M2 muscarinic acetylcholine receptors.<sup>7,22</sup> Our data to this point suggest that the conducting role for  $K_v2.1$  is minimal in the absence of muscarinic activation. To assess whether  $K_v2.1$  conductances play a role in mediating the effects of C-boutons, we proceeded to compare motoneuron responses to muscarine in control and ChAT- $K_v2.1^{OFF}$  mice.

In neonatal motoneurons, exogenously applied muscarine has mixed effects due to the different subtypes (M2/M3) of receptors.<sup>44</sup> In agreement with those findings, we found that P2-P7 motoneurons ( $n = 9$ ) had large depolarizations in response to muscarine (10  $\mu$ M). However, in motoneurons from P13 and older mice ( $n = 10$ ), muscarine did not affect resting membrane potential ([Figure S4](#)). Rather, the effects of muscarine were dominated by those shown to be due to M2 receptor activation<sup>3</sup> as outlined in the following text.

Perfusion of mature control and ChAT- $K_v2.1^{OFF}$  motoneurons with 10  $\mu$ M muscarine had little effect on AP amplitude ([Figures S4C and S4D](#)), 1/2-width ([Figure S4E](#)), or fAHP amplitude ([Figure S4F](#)). However, the mAHP amplitude ([Figure S4G](#)) and 1/2-decay time ([Figure S4H](#)) were significantly decreased in both control and ChAT- $K_v2.1^{OFF}$  motoneurons.

In agreement with previous work in control motoneurons,<sup>3</sup> and in line with the reduction in mAHP conductances, muscarine affected firing of mature motoneurons from both ChAT- $K_v2.1^{OFF}$  ([Figure 5A](#)) and  $K_v2.1^{ON}$  ([Figure 5B](#)) mice. Muscarine increased overall  $f$ -I slope ([Figures 5A–5D](#)), but not the  $f$ -I slope of the first interval ([Figure 5E](#)), and induced moderate increases in maximum overall firing frequency ([Figure 5F](#)). The first spike interval frequency was not altered by muscarine ([Figure 5G](#)). That is, the absence of  $K_v2.1$  channels did not affect motoneuron responsiveness to muscarine.

As  $K_v2$  channels have been shown in other neurons to prevent depolarizing block to maintain firing during high synaptic drive, we asked whether muscarinic receptor activation might modulate  $K_v2.1$  to increase the current threshold at which spike output is blocked. However, muscarine had no effect on depolarizing block threshold in either control or cKO motoneurons ([Figure 5H](#)).

Taken together, these results show that  $K_v2.1$  is not required for muscarine-evoked increases in motoneuron excitability.

**Motor behavior and C-bouton amplification is preserved in ChAT- $K_v2.1^{OFF}$  mice**

Despite our *in vitro* data showing  $K_v2.1$  channels are not necessary for motoneuron amplification (including following muscarine application), we tested whether our negative electrophysiology results translated to behavior, i.e., whether ChAT- $K_v2.1^{OFF}$  mice would show deficits in high force tasks. Voluntary motor behavior over a chronic period was assessed by individually housing male ([Figure S5A](#)) and female ([Figure S5B](#)) mice of both genotypes in cages with *ad libitum* access to a running wheel for either 23 days (males) or 32 days (females). Male control and ChAT- $K_v2.1^{OFF}$  mice ran similar daily distances throughout the 23 day period. We recorded females for a longer duration as their distances (which are much greater than males) seemed to change over the course of 5 weeks. Although at no time point were the female ChAT- $K_v2.1^{OFF}$  significantly different from control mice, the control mice—unlike their male counterparts—seemed to increase their running distances over time, with the slope over five weeks being significantly greater than that of ChAT- $K_v2.1^{OFF}$  mice ( $p = 0.003$ ).

We next examined the running capacity of mice on a treadmill inclined 15° to increase locomotor force demands. The maximum speed for male ChAT- $K_v2.1^{OFF}$  group was on average 13% (6 cm/s) slower than control mice. Although the effect size was large, the 95% confidence interval was wide and crossed 0 ( $CI_{95} = [-1.84, 0.07]$ ), indicating a relatively low degree of certainty in the magnitude of this effect ([Figure S5C](#)). There was no difference in this measure for female mice ([Figure S5F](#)).

Other behavioral measures, including the maximum distance run at 60% of maximum speed ([Figures S5D and S5G](#)) and grip strength ([Figures S5E and S5H](#)), were similar in both genotypes for male ([Figures S5D and S5E](#)) and female ([Figures S5G and S5H](#)) mice.

In short, we were unable to detect any significant deficits in either male or female ChAT- $K_v2.1^{OFF}$  mice using these particular tasks.

C-bouton mediated amplification can be specifically assessed *in vivo* by comparing EMG amplitudes during walking and swimming: when C-bouton synaptic transmission is genetically perturbed, the ratio of the EMG amplitude during swimming vs. walking is reduced compared

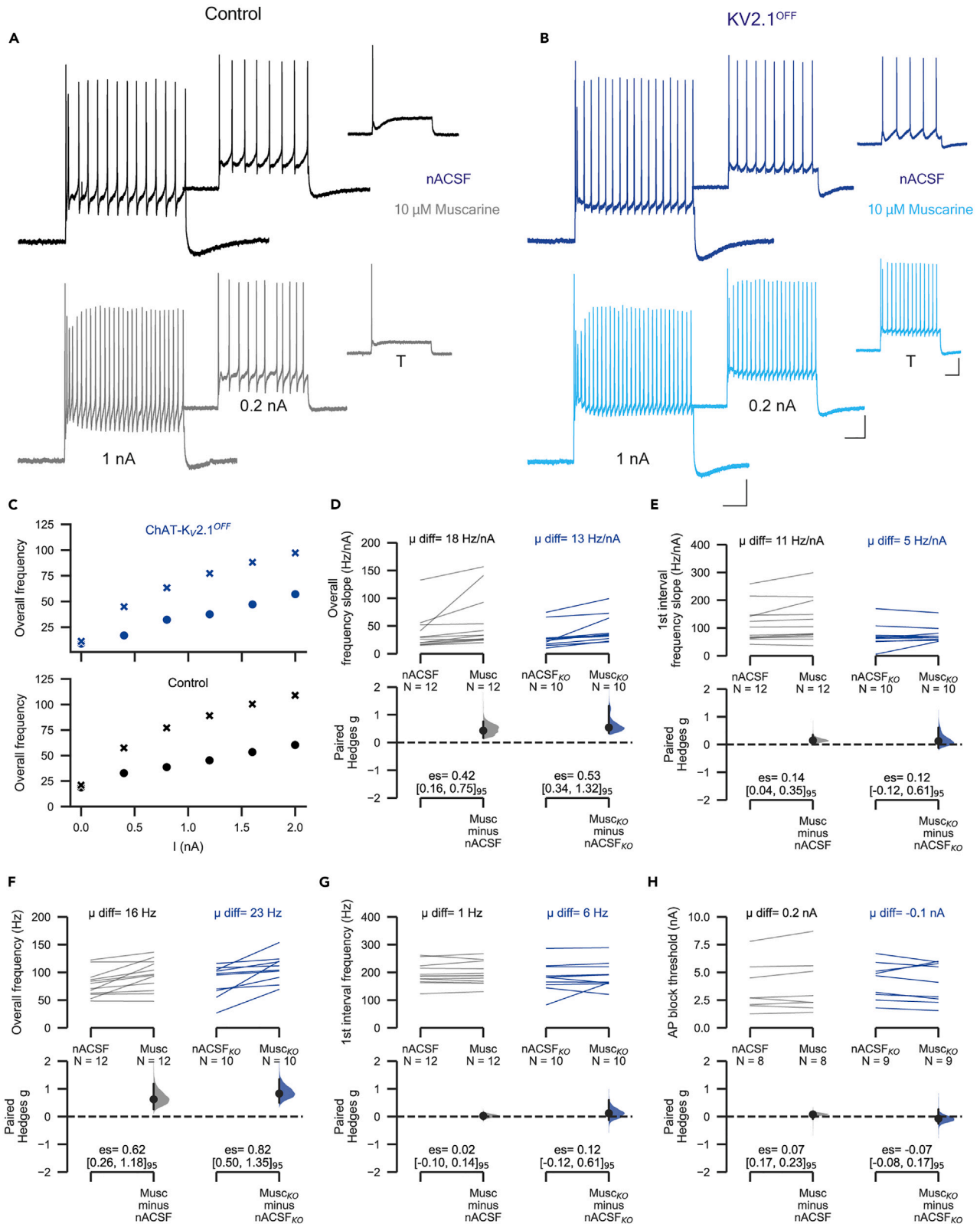


**Figure 5. Muscarinic induced increase in excitability is preserved in ChAT-K<sub>v</sub>2.1<sup>OFF</sup> motoneurons**

See also Figures S4 and S5.

(A and B) The changes in firing characteristics following perfusion with 10 μM muscarine were compared for motoneurons of control (A) and ChAT-K<sub>v</sub>2.1<sup>OFF</sup> mice (B). Representative traces at threshold (T), 0.2 nA and 1 nA above threshold before (nACSF, black and dark blue traces) and after perfusion with muscarine (10 μM, gray and sky blue).

(C) Scatterplots showing the overall frequency in response to increasing current inputs in control (upper) and ChAT-K<sub>v</sub>2.1<sup>OFF</sup> (lower) motoneurons (circles control, x muscarine).

(D–H) Paired Hedges g for overall frequency slope (D), 1<sup>st</sup> interval frequency slope (E), maximum overall frequency (F), maximum 1<sup>st</sup> interval frequency (G), and AP block threshold (H) in control (left) and ChAT-K<sub>v</sub>2.1<sup>OFF</sup> (right) motoneurons are shown in Cumming paired estimation plots. Experimental unit (N) = motoneurons. Number of animals used was as follows: control = 8 (2 females, 6 males), ChAT-K<sub>v</sub>2.1<sup>OFF</sup> = 6 (2 females, 4 males). Scale bars in A and B: horizontal, 100 ms, vertical, 20 mV. Mean difference is abbreviated to “μ diff”, and hedges g estimation statistic is represented by “es”. See also Figure S4.

to mice with functional C-bouton signaling.<sup>4,45,46</sup> Thus, if K<sub>v</sub>2.1 were critical to C-bouton function, a similar decrease in motor amplification would be expected following K<sub>v</sub>2.1 cKO in motoneurons. However, we found no difference in EMG amplification during swimming between control and ChAT-K<sub>v</sub>2.1<sup>OFF</sup> female mice in either the extensor medial gastrocnemius (MG) muscle (Figures 6A–6A2) or the flexor tibialis anterior (TA) muscle (Figures 6B–6B2, male mice were not studied).

In summary, the only behavioral effect of eliminating K<sub>v</sub>2.1 from cholinergic neurons that we observed was that of a possible training effect in female mice given *ad libitum* access to a running wheel. Notably, these data suggest that either K<sub>v</sub>2.1 channels are not necessary for motoneuron amplification—the key reported role of C-boutons—or that their absence can be compensated to maintain behavioral homeostasis.

**K<sub>v</sub>2.2 is expressed in the spinal cord and co-localizes with K<sub>v</sub>2.1 opposite to C-boutons**

The lack of behavioral deficits, particularly in motoneuron amplification following cKO of K<sub>v</sub>2.1 were surprising findings considering that these channels are prominent at all C-bouton synapses and thought to be an integral part of the synaptic machinery.<sup>21,22</sup> Although K<sub>v</sub>2.1 is considered to be the predominant K<sub>v</sub>2 subunit in motoneurons, in many brain neurons K<sub>v</sub>2.1 subunits share some functional homology and are co-expressed with K<sub>v</sub>2.2 subunits.<sup>29,35,39–41</sup> We therefore proceeded with immunohistochemistry experiments to identify whether K<sub>v</sub>2.2 is also expressed in motoneurons. We found that K<sub>v</sub>2.2 puncta were abundant in the spinal cord and often but not always co-localized with K<sub>v</sub>2.1 (Figures S6A–S6F). In the dorsal horn (Figures S6A–S6C1), K<sub>v</sub>2.1 was predominantly expressed in the deeper laminae, whereas K<sub>v</sub>2.2 positive cells were concentrated in the superficial laminae. In the deep dorsal/intermediate laminae (Figures S6D–S6F1), K<sub>v</sub>2.2 expression was mostly confined to medial regions, and as well as forming large clusters on somata, an area of smaller, more diffuse puncta was located lateral to the dorsal columns (Figures S6D–S6F1). In the same region, K<sub>v</sub>2.1 puncta were distributed across the medio-lateral axis, mainly in neurons without K<sub>v</sub>2.2 labeling. In the ventral horn (Figures 7A–7F), K<sub>v</sub>2.2 seemed to be exclusively confined to motoneurons, where labeling was co-localized with K<sub>v</sub>2.1. Co-labeling experiments with ChAT confirmed that indeed K<sub>v</sub>2.2 clusters are opposed to C-boutons (Figures 7D–7F). Thus, K<sub>v</sub>2.2 channels are clearly co-localized with K<sub>v</sub>2.1 channels at motoneuron membranes in apposition to pre-synaptic C-boutons.

**DISCUSSION**

K<sub>v</sub>2.1 channels are expressed by spinal motoneurons where they largely aggregate opposite C-bouton synapses,<sup>7</sup> clustering in the post-natal period as the motor system matures.<sup>8,43,47,48</sup> K<sub>v</sub>2.1 delayed rectifier currents have been implicated as crucial regulators of motoneuron firing and C-bouton amplification of motor output. Here, we show that K<sub>v</sub>2.1 does not regulate firing in mature motoneurons. Furthermore, in the absence of K<sub>v</sub>2.1 channels in motoneurons, C-bouton amplification of motor output during behavior is preserved. We also show that motoneurons co-express K<sub>v</sub>2.2 and suggest that K<sub>v</sub>2 channels function as non-conducting proteins in mature motoneurons. Thus, our data challenge current concepts of motoneuron physiology and raise new questions about the role of these prominent channels in motoneuron behavior.

**Co-expression of K<sub>v</sub>2.1 and K<sub>v</sub>2.2 in motoneurons**

The structure and function of neuronal K<sub>v</sub>2 channels has been studied for over 3 decades, since K<sub>v</sub>2.1 was shown to be expressed in rat brain.<sup>12</sup> K<sub>v</sub>2.2 channels were discovered shortly afterward, and, although the two subtypes have similar electrophysiological properties, substantial differences in their expression profiles across the brain were initially reported.<sup>13</sup> In addition to their expression being in different neurons, K<sub>v</sub>2.2 (initially called “CDRK”) expression seemed to be restricted to neuronal processes rather than somata.<sup>14</sup> The prominence of K<sub>v</sub>2.1 expression led these channels to become the primary focus of further studies of K<sub>v</sub>2 regulation of neuronal excitability.

However, this characterization of K<sub>v</sub>2.2 was based on an unfortunate cloning error, and it was later demonstrated that both K<sub>v</sub>2 isoforms are “co-localized in the somata and proximal dendrites of cortical pyramidal neurons and are capable of forming heteromeric channels”.<sup>49</sup> Nonetheless, much of the focus has remained on K<sub>v</sub>2.1 and only recently has K<sub>v</sub>2.2 received increasing attention.<sup>29,30,39,40,49</sup> But K<sub>v</sub>2.2 has remained largely unexplored in motoneurons (see Stewart et al.).<sup>50</sup> Here, we show that K<sub>v</sub>2.2 is also expressed post-synaptically to C-boutons, is co-clustered with K<sub>v</sub>2.1, and as such, should be taken into consideration when investigating C-bouton function. Whether K<sub>v</sub>2.2 expression increases in ChAT-K<sub>v</sub>2.1<sup>OFF</sup> motoneurons as a compensatory mechanism remains unknown.

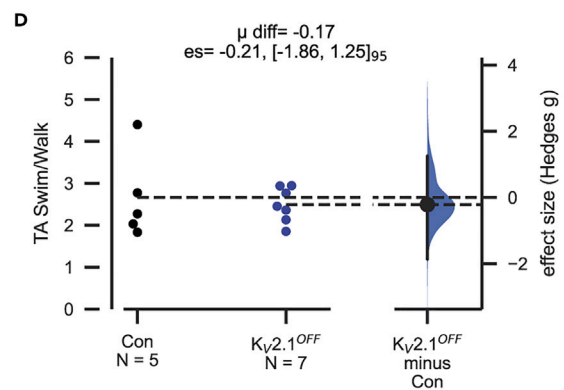
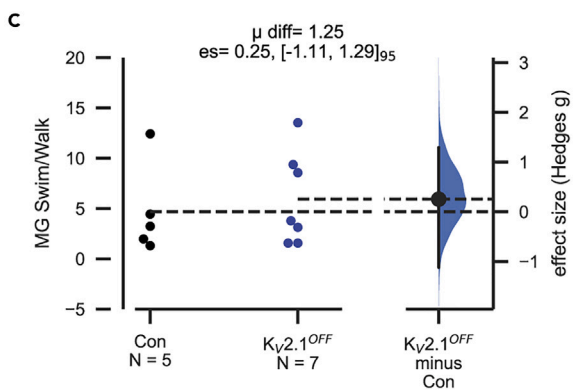
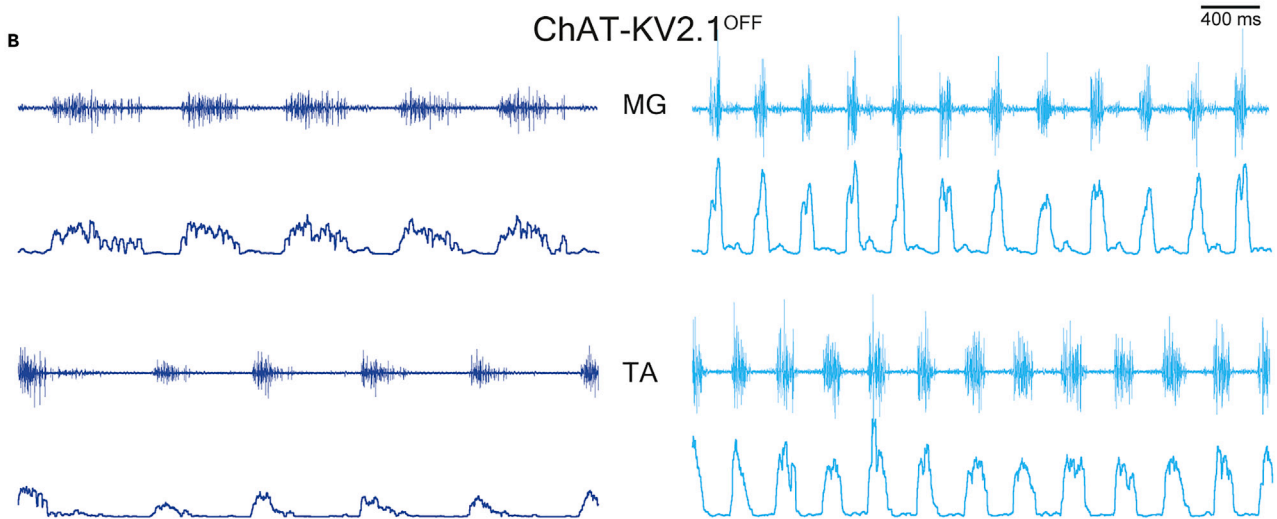
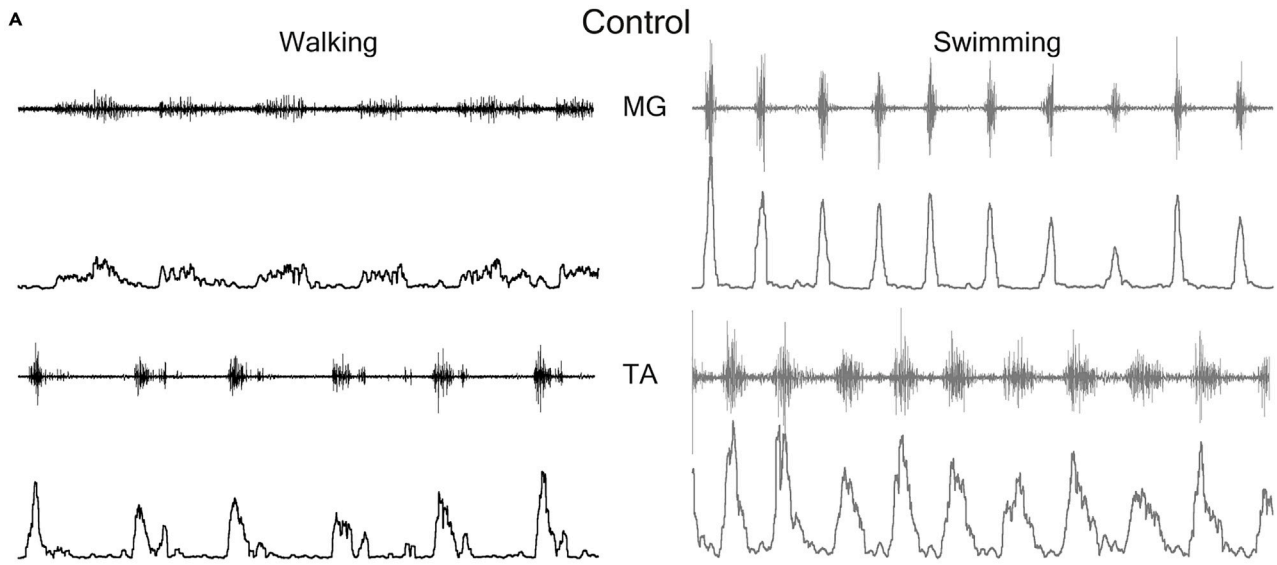


**Figure 6. Motor behavior and C-bouton amplification is preserved in ChAT-K<sub>v</sub>2.1<sup>OFF</sup> mice**

See also Figure S5.

(A and B) Representative medial gastrocnemius (MG) and tibialis anterior (TA) EMG traces from a control (A) and ChAT-K<sub>v</sub>2.1<sup>OFF</sup> mouse (B). For control mice (A), black traces are those recorded during walking at 0.15 m/s and gray traces are during swimming. In ChAT-K<sub>v</sub>2.1<sup>OFF</sup> mice (B), blue traces are walking at 0.15 m/s and sky blue is swimming. For each muscle, top traces are raw EMGs and lower traces are corresponding RMS amplitudes.

(C and D) Gardner-Altman estimation plots for MG and TA. Experimental unit (N) = animals, all were females. Mean difference is abbreviated to “μ diff”, and hedges g estimation statistic is represented by “es”. See also Figure S5.

**Reconciling differences with studies of K<sub>v</sub>2.1 function in immature motoneurons**

Our experiments were initially performed with the assumption that K<sub>v</sub>2.1 was the predominant K<sub>v</sub>2 subtype in motoneurons and that it had a significant conducting role. We were therefore surprised to find that the only difference in mature ChAT-K<sub>v</sub>2.1<sup>OFF</sup> motoneurons compared to controls was a capacity to fire at higher rates. The reason for these higher firing rates is not clear, but they may be due to disruption of the post-synaptic site (see in the following text). But given the filtering properties of muscle fibers, these high-sustained frequencies may not be relevant to muscle contraction (Enoka and Farina, 2021).

If K<sub>v</sub>2 channels were to have an electrical role, acute inhibition with GxTX-1E would significantly alter firing characteristics of both control (K<sub>v</sub>2.1<sup>ON</sup>/K<sub>v</sub>2.2<sup>ON</sup>) and ChAT-K<sub>v</sub>2.1<sup>OFF</sup> motoneurons (ChAT-K<sub>v</sub>2.1<sup>OFF</sup>/K<sub>v</sub>2.2<sup>ON</sup>), as it did in wild-type pyramidal neurons. However, the only consistent effect we found in response to toxin was a relatively small (less than 10% in all neurons) reduction in the instantaneous frequency of the initial two spikes in a train. We saw the same effect in ChAT-K<sub>v</sub>2.1<sup>OFF</sup> motoneurons, suggesting K<sub>v</sub>2.2 currents also contribute to maintaining high initial firing frequencies. Functionally, this could be significant as small increases in initial firing frequencies are known to significantly increase the rate of muscle force production.

We note that these findings contrast with those indicating that K<sub>v</sub>2 inhibition alters motoneuron firing and excitability.<sup>20–22</sup> Fletcher et al. (2017) used GxTX-1E to block motoneuron K<sub>v</sub>2 channels in P4 mice, suggesting that K<sub>v</sub>2 conductances maintain narrow spikes and repetitive firing at low current inputs and increase firing frequencies. Romer et al. (2019) assessed the contribution of K<sub>v</sub>2 to regulation of motoneuron firing in spinal cord slices from P8–12 rats, which are approaching motor maturity. They reported that blocking K<sub>v</sub>2 channels with stromatoxin led to unsustainability of repetitive firing, a reduction in excitability (f-I slope), and a slowing of the rising and falling phases of action potentials (similar to Fletcher et al., 2017). And Nascimento et al. (2020) showed in young (P2–P7) motoneurons that chemogenetic activation of V0<sub>C</sub> interneurons (the neuronal source of C-boutons) decreases spike width, while increasing maximal firing rates, the current required for depolarizing block, and mAHP; these effects were all blocked by GxTX-1E. They thus suggested that clustered K<sub>v</sub>2.1 channels underlie these M2-mediated electrophysiological effects and are recruited by C-boutons for motor amplification.

Our results in young motoneurons are in keeping with the aforementioned studies. For example, we too showed that K<sub>v</sub>2 channels contribute to spike width in early post-natal life, during a period when K<sub>v</sub>2.1 channels and motor control are immature.<sup>8,43</sup> But this contribution is minimal in mature motoneurons. And the one study aforementioned in an intermediate developmental stage (Romer et al., 2019) used stromatoxin, which blocks K<sub>v</sub>2 channels but also has off target effects (K<sub>v</sub>4.2 channels with a low IC<sub>50</sub>) that make interpretation of current clamp data challenging.<sup>34,51</sup>

Another difference between our study and that of Nascimento et al. (2020) is the specificity of C-bouton activation. While their chemogenetic activation would limit off target effects, we used muscarine—an agonist of all muscarinic receptors that has been shown to have mixed effects on early post-natal motoneurons.<sup>3,44</sup> Indeed, we found that in young motoneurons, muscarine led to significant depolarizations.<sup>52</sup> But these effects were not present beyond the 2<sup>nd</sup> post-natal week, suggesting a change in muscarine receptor effects. In these older motoneurons, the effects we report with muscarine were dominated by M2-/C-bouton-type effects of increased excitability, and these were similar in ChAT-K<sub>v</sub>2.1<sup>OFF</sup> and K<sub>v</sub>2.1<sup>ON</sup> motoneurons.

It therefore seems most likely that the differences in findings between the aforementioned studies and ours can be reconciled by considering the maturity of the preparations and the specificity of GxTX-1E for K<sub>v</sub>2 channels.

**A potential non-conducting role for K<sub>v</sub>2 channels at C-bouton synapses**

Given that muscarine increased excitability in ChAT-K<sub>v</sub>2.1<sup>OFF</sup> motoneurons despite the absence of K<sub>v</sub>2.1 channels, and our behavioral data showed that ChAT-K<sub>v</sub>2.1<sup>OFF</sup> mice could normally amplify their motor output, it is likely that K<sub>v</sub>2.1 channels are not necessary for M2 receptor-mediated motor amplification by C-boutons. Our finding that K<sub>v</sub>2.2 channels are co-expressed with K<sub>v</sub>2.1 at C-bouton synapses suggests that if K<sub>v</sub>2 channels are important for neuronal function, K<sub>v</sub>2.2 can function independently of K<sub>v</sub>2.1 during behaviors requiring C-bouton activation.

We propose that K<sub>v</sub>2 channels have a minimally conducting role in mature motoneurons. That is, we suggest that in motoneurons, K<sub>v</sub>2 channels have a primarily non-canonical function.<sup>27,30,32,33,53–56</sup>

What role might K<sub>v</sub>2 channels play at C-bouton synapses? K<sub>v</sub>2 channels in the PM form physical links with the ER membrane via VAP proteins, creating tight EJPs.<sup>9,28–30</sup> There is growing evidence in central neurons and smooth muscle suggesting that K<sub>v</sub>2.1 is responsible for the spatial and functional coupling of channels such as L-type calcium channels and RyRs into a Ca<sup>2+</sup>-signaling microdomain. Although it does not seem that RyRs are expressed at C-bouton synapses, there are several different proteins apposing C-boutons that are Ca<sup>2+</sup>-dependent (such as SK2/3), leading to the suggestion that K<sub>v</sub>2 channels may serve a role in the regulation of these proteins in motoneurons.<sup>55,57</sup> Given that K<sub>v</sub>2.1 knockout did not have an effect on C-bouton function, it is unlikely that other C-bouton components

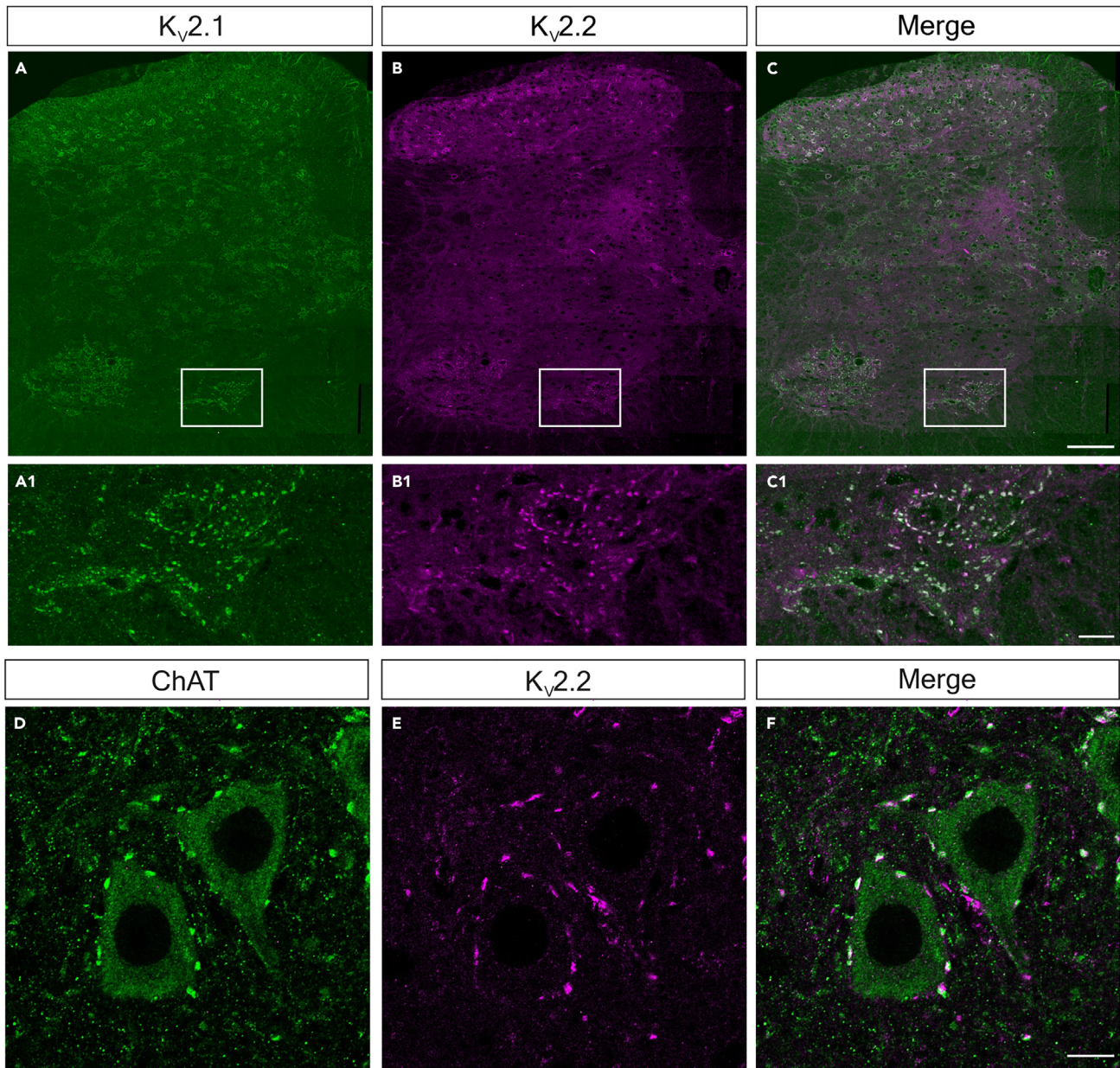


**Figure 7.  $K_v2.2$  is expressed in the spinal cord and co-localizes with  $K_v2.1$  opposite to C-boutons**

See also [Figure S6](#).

(A–C) 40 $\times$  confocal tiled, z stack projection images ( $5 \times 1 \mu\text{m}$  slices) of the lumbar spinal cord stained for  $K_v2.1$  (A) and  $K_v2.2$  (B); merged image shown in (C). (A1–C1) Boxes depicted in A–C, expanded.

(D–F) 40 $\times$  confocal single optical sections showing  $K_v2.2$  (D) expression opposite VACHT<sup>+</sup> C-boutons (E), with a merge of both channels in (F). Scale bars in (A–C), 80  $\mu\text{m}$ , (A1–C1), 25  $\mu\text{m}$ , (D–F), 10  $\mu\text{m}$ . See also [Figure S7](#).

were affected. We therefore suggest that  $K_v2.2$  channels serve a similar role and can subsume the non-conducting roles of  $K_v2.1$ . Further studies using double knock out experiments could determine the combined roles of  $K_v2$  channels in motoneuron and C-bouton physiology.

Evolution led to the development of C-bouton synapses to amplify motor output in a task-dependent manner.<sup>3,4</sup> To understand the mechanisms of this important amplification, it is necessary to identify the structure and function of the plethora of proteins clustered in this region and to understand how these proteins interact with each other. We demonstrate that in motoneurons, post-synaptic  $K_v2.1$  and  $K_v2.2$  are

co-expressed and likely serve predominantly non-conducting roles. However, the data also highlight that there is still much to learn regarding synaptic mechanisms of C-bouton motor amplification.

### Limitations of the study

Here, we targeted the largest motoneurons, reasoning that C-bouton amplification is principally evident in high-motor output tasks<sup>4</sup> and is thus related to recruitment of the faster (and larger) motoneurons that innervate higher force-producing fast-twitch muscle fibers. In fast vs. slow mouse motoneurons, there are differences in the expression of channels that contribute to membrane voltage bistability, including Nav1.6, Trpm5, and Kv1.2.<sup>58</sup> Fast motoneurons have a higher density of C-boutons<sup>59</sup>; it is possible that there are clustering/expression differences in Kv2 channels at these sites between slow and fast motoneurons, although none have been reported. In any case, taking the electrophysiological data together with the behavioral data together with the known high density of C-boutons on motoneurons, it is unlikely that a bias toward the larger motoneurons significantly impacted our conclusions.

### STAR★METHODS

Detailed methods are provided in the online version of this paper and include the following:

- KEY RESOURCES TABLE
- RESOURCE AVAILABILITY
  - Lead contact
  - Materials availability
  - Data and code availability
- EXPERIMENTAL MODEL AND STUDY PARTICIPANTS
  - Animals
  - Blinding and randomisation
- METHOD DETAILS
  - Immunohistochemistry
  - Patch clamp electrophysiology
  - EMG recording for C-bouton motor amplification
  - Behavioural assessments and analysis
- QUANTIFICATION AND STATISTICAL ANALYSIS

### SUPPLEMENTAL INFORMATION

Supplemental information can be found online at <https://doi.org/10.1016/j.isci.2024.110444>.

### ACKNOWLEDGMENTS

This work was supported by a Wellcome Investigator Award (110193/Z/15/Z) to R.B., and a Biotechnology and Biological Sciences Research Council Research Grant (BB/S005943/1) to M.B. R.B. is supported by Brain Research UK, and F.N. is supported by a Sir Henry Wellcome Post-doctoral Fellowship 221610/Z/20/Z.

We thank Amanda Pocratsky for the graphical abstract, Shireen Salem for help with staining and imaging of spinal cord slices for development experiments, and Nadine Simons-Weidenmaier for technical assistance and managing mouse colonies.

### AUTHOR CONTRIBUTIONS

R.M.B. conceived the study. C.C.S. and R.M.B. designed the study. C.C.S. acquired and analyzed the data. F.N. and G.O. performed and analyzed the voltage clamp experiments. C.C.S., M.B., and R.M.B. interpreted the data and wrote the paper. All authors approved the final version of the manuscript, agree to be accountable for all aspects of the work, and confirm that all those who qualify for authorship are listed.

### DECLARATION OF INTERESTS

R.M.B. is a co-founder, board member, and consultant to Sania Therapeutics, Inc, an early stage gene therapy company, and CCS is now working for Sania. The work presented here is from the Brownstone UCL lab and has no financial implications for Sania.

Received: February 9, 2024

Revised: April 29, 2024

Accepted: July 1, 2024

Published: July 3, 2024



REFERENCES

- Enoka, R.M., and Farina, D. (2021). Force steadiness: From motor units to voluntary actions. *Physiology* 36, 114–130. <https://doi.org/10.1152/PHYSIOL.00027.2020/ASSET/IMAGES/LARGE/AJ-PHYS200009F006.JPEG>.
- Conradi, S. (1969). Ultrastructure and distribution of neuronal and glial elements on the surface of the proximal part of a motoneuron dendrite, as analyzed by serial sections. *Acta Physiol. Scand. Suppl.* 332, 49–64.
- Miles, G.B., Hartley, R., Todd, A.J., and Brownstone, R.M. (2007). Spinal cholinergic interneurons regulate the excitability of motoneurons during locomotion. *Proc. Natl. Acad. Sci. USA* 104, 2448–2453. <https://doi.org/10.1073/pnas.061134104>.
- Zagoraiou, L., Akay, T., Martin, J.F., Brownstone, R.M., Jessell, T.M., and Miles, G.B. (2009). A Cluster of Cholinergic Premotor Interneurons Modulates Mouse Locomotor Activity. *Neuron* 64, 645–662. <https://doi.org/10.1016/j.neuron.2009.10.017>.
- Hellström, J., Oliveira, A.L.R., Meister, B., and Cullheim, S. (2003). Large cholinergic nerve terminals on subsets of motoneurons and their relation to muscarinic receptor type 2. *J. Comp. Neurol.* 460, 476–486. <https://doi.org/10.1002/cne.10648>.
- Deardorff, A.S., Romer, S.H., Deng, Z., Bullinger, K.L., Nardelli, P., Cope, T.C., and Fyffe, R.E.W. (2013). Expression of postsynaptic Ca<sup>2+</sup>-activated K<sup>+</sup> (SK) channels at C-bouton synapses in mammalian lumbar  $\alpha$ -motoneurons. *J. Physiol.* 591, 875–897. <https://doi.org/10.1113/jphysiol.2012.240879>.
- Muennich, E.A.L., and Fyffe, R.E.W. (2004). Focal aggregation of voltage-gated, Kv2.1 subunit-containing, potassium channels at synaptic sites in rat spinal motoneurons. *J. Physiol.* 554, 673–685. <https://doi.org/10.1113/JPHYSIOL.2003.056192>.
- Wilson, J.M., Rempel, J., and Brownstone, R.M. (2004). Postnatal development of cholinergic synapses on mouse spinal motoneurons. *J. Comp. Neurol.* 474, 13–23. <https://doi.org/10.1002/CNE.20089>.
- Deardorff, A.S., Romer, S.H., and Fyffe, R.E.W. (2021). Location, location, location: the organization and roles of potassium channels in mammalian motoneurons. *J. Physiol.* 599, 1391–1420. <https://doi.org/10.1113/JP278675>.
- Romer, S.H., Dominguez, K.M., Gelpi, M.W., Deardorff, A.S., Tracy, R.C., and Fyffe, R.E.W. (2014). Redistribution of Kv<sub>2.1</sub> ion channels on spinal motoneurons following peripheral nerve injury. *Brain Res.* 1547, 1–15.
- Trimmer, J.S. (1991). Immunological identification and characterization of a delayed rectifier K<sup>+</sup> channel polypeptide in rat brain. *Proc. Natl. Acad. Sci. USA* 88, 10764–10768. <https://doi.org/10.1073/PNAS.88.23.10764>.
- Frech, G.C., VanDongen, A.M.J., Schuster, G., Brown, A.M., and Joho, R.H. (1989). A novel potassium channel with delayed rectifier properties isolated from rat brain by expression cloning. *Nature* 340, 642–645. <https://doi.org/10.1038/340642a0>.
- Hwang, P.M., Glatt, C.E., Bredt, D.S., Yellen, G., and Snyder, S.H. (1992). A novel K<sup>+</sup> channel with unique localizations in mammalian brain: Molecular cloning and characterization. *Neuron* 8, 473–481. [https://doi.org/10.1016/0896-6273\(92\)90275-1](https://doi.org/10.1016/0896-6273(92)90275-1).
- Hwang, P.M., Cunningham, A.M., Peng, Y.W., and Snyder, S.H. (1993). CDRK and DRK1 K<sup>+</sup> channels have contrasting localizations in sensory systems. *Neuroscience* 55, 613–620. [https://doi.org/10.1016/0306-4522\(93\)90427-H](https://doi.org/10.1016/0306-4522(93)90427-H).
- Hwang, P.M., Fotuhi, M., Bredt, D.S., Cunningham, A.M., and Snyder, S.H. (1993). Contrasting immunohistochemical localizations in rat brain of two novel K<sup>+</sup> channels of the Shab subfamily. *J. Neurosci.* 13, 1569–1576. <https://doi.org/10.1523/jneurosci.13-04-01569.1993>.
- Jegla, T., Marlow, H.Q., Chen, B., Simmons, D.K., Jacobo, S.M., and Martindale, M.Q. (2012). Expanded Functional Diversity of Shaker K<sup>+</sup> Channels in Cnidarians Is Driven by Gene Expansion. *PLoS One* 7, e51366. <https://doi.org/10.1371/JOURNAL.PONE.0051366>.
- Torkamani, A., Bersell, K., Jorge, B.S., Bjork, R.L., Friedman, J.R., Bloss, C.S., Cohen, J., Gupta, S., Naidu, S., Vanoye, C.G., et al. (2014). De novo KCNB1 mutations in epileptic encephalopathy. *Ann. Neurol.* 76, 529–540. <https://doi.org/10.1002/ANA.24263>.
- Thiffault, I., Speca, D.J., Austin, D.C., Cobb, M.M., Eum, K.S., Safina, N.P., Grote, L., Farrow, E.G., Miller, N., Soden, S., et al. (2015). A novel epileptic encephalopathy mutation in KCNB1 disrupts Kv2.1 ion selectivity, expression, and localization. *J. Gen. Physiol.* 146, 399–410. <https://doi.org/10.1085/JGP.201511444>.
- Speca, D.J., Ogata, G., Mandikian, D., Bishop, H.I., Wiler, S.W., Eum, K., Wenzel, H.J., Doisy, E.T., Matt, L., Campi, K.L., et al. (2014). Deletion of the Kv2.1 delayed rectifier potassium channel leads to neuronal and behavioral hyperexcitability. *Genes Brain Behav.* 13, 394–408. <https://doi.org/10.1111/GBB.12120>.
- Fletcher, E.V., Simon, C.M., Pagiazitis, J.G., Chalif, J.I., Vukojicic, A., Drobac, E., Wang, X., and Mentis, G.Z. (2017). Reduced sensory synaptic excitation impairs motor neuron function via Kv2.1 in spinal muscular atrophy. *Nat. Neurosci.* 20, 905–916. <https://doi.org/10.1038/NN.4561>.
- Romer, S.H., Deardorff, A.S., Fyffe, R.E.W., Forsythe, I., Murrell-Lagnado, R., and Romer, S.H. (2019). A molecular rheostat: Kv2.1 currents maintain or suppress repetitive firing in motoneurons. *J. Physiol.* 597, 3769–3786. <https://doi.org/10.1113/JP277833>.
- Nascimento, F., Broadhead, M.J., Tetranga, E., Tsape, E., Zagoraiou, L., and Miles, G.B. (2020). Synaptic mechanisms underlying modulation of locomotor-related motoneuron output by premotor cholinergic interneurons. *Elife* 9, e54170. <https://doi.org/10.7554/eLife.54170>.
- Dixon, R.E., and Trimmer, J.S. (2022). Endoplasmic Reticulum–Plasma Membrane Junctions as Sites of Depolarization-Induced Ca<sup>2+</sup> Signaling in Excitable Cells. *Annu. Rev. Physiol.* 85, 217–243. <https://doi.org/10.1146/annurev-physiol-032122-10461085>.
- Maverick, E.E., and Tamkun, M.M. (2022). High spatial density is associated with non-conducting Kv channels from two families. *Biophys. J.* 121, 755–768. <https://doi.org/10.1016/j.bpj.2022.01.021>.
- O’Connell, K.M.S., Loftus, R., and Tamkun, M.M. (2010). Localization-dependent activity of the Kv2.1 delayed-rectifier K<sup>+</sup> channel. *Proc. Natl. Acad. Sci. USA* 107, 12351–12356. <https://doi.org/10.1073/PNAS.1003028107/-DCSUPPLEMENTAL/PNAS.201003028SI.PDF>.
- Fox, P.D., Loftus, R.J., and Tamkun, M.M. (2013). Cellular/Molecular Regulation of Kv2.1 K Conductance by Cell Surface Channel Density. *J. Neurosci.* 33, 1259–1270. <https://doi.org/10.1523/JNEUROSCI.3008-12.2013>.
- Matsumoto, C., O’dwyer, S.C., Manning, D., Hernandez-Hernandez, G., Rhana, P., Fong, Z., Sato, D., Clancy, C.E., Vierra, N.C., Trimmer, J.S., and Fernando Santana, L. (2023). The formation of Kv2.1 macro-clusters is required for sex-specific differences in L-type Cav1.2 clustering and function in arterial myocytes. *Commun. Biol.* 6, 1165. <https://doi.org/10.1038/s42003-023-05527-1>.
- Fox, P.D., Haberkorn, C.J., Akin, E.J., Seel, P.J., Krapf, D., and Tamkun, M.M. (2015). Induction of stable ER-plasma-membrane junctions by Kv2.1 potassium channels. *J. Cell Sci.* 128, 2096–2105. <https://doi.org/10.1242/JCS.166009/VIDEO-1>.
- Johnson, B., Leek, A.N., Solé, L., Maverick, E.E., Levine, T.P., and Tamkun, M.M. (2018). Kv2 potassium channels form endoplasmic reticulum/plasma membrane junctions via interaction with VAPA and VAPB. *Proc Natl Acad Sci USA* 115, E7331–E7340. <https://doi.org/10.1073/pnas.1805757115>.
- Kirmiz, M., Vierra, N.C., Palacio, S., and Trimmer, J.S. (2018). Identification of VAPA and VAPB as Kv2 channel-interacting proteins defining endoplasmic reticulum–plasma membrane junctions in mammalian brain neurons. *J. Neurosci.* 38, 7562–7584. <https://doi.org/10.1523/JNEUROSCI.0893-18.2018>.
- O’Dwyer, S.C., Palacio, S., Matsumoto, C., Guarina, L., Klug, N.R., Tajada, S., Rosati, B., McKinnon, D., Trimmer, J.S., and Santana, L.F. (2020). Kv2.1 channels play opposing roles in regulating membrane potential, Ca<sup>2+</sup> channel function, and myogenic tone in arterial smooth muscle. *Proc. Natl. Acad. Sci. USA* 117, 3858–3866. [https://doi.org/10.1073/PNAS.1917879117/SUPPL\\_FILE/PNAS.1917879117.SAPP.PDF](https://doi.org/10.1073/PNAS.1917879117/SUPPL_FILE/PNAS.1917879117.SAPP.PDF).
- Vierra, N.C., Ribeiro-Silva, L., Kirmiz, M., Van Der List, D., Bhandari, P., Mack, O.A., Carroll, J., Le Monnier, E., Aicher, S.A., Shigemoto, R., and Trimmer, J.S. (2023). Neuronal ER-plasma membrane junctions couple excitation to Ca<sup>2+</sup>-activated PKA signaling. *Nat. Commun.* 14, 5231. <https://doi.org/10.1038/s41467-023-40930-6>.
- Vierra, N.C., Kirmiz, M., van der List, D., Santana, L.F., and Trimmer, J.S. (2019). Kv2.1 mediates spatial and functional coupling of L-type calcium channels and ryanodine receptors in mammalian neurons. *Elife* 8, e49953. <https://doi.org/10.7554/ELIFE.49953>.
- Liu, P.W., and Bean, B.P. (2014). Kv2 channel regulation of action potential repolarization and firing patterns in superior cervical ganglion neurons and hippocampal CA1 pyramidal neurons. *J. Neurosci.* 34, 4991–5002. <https://doi.org/10.1523/JNEUROSCI.1925-13.2014>.
- Kimm, T., Khaliq, Z.M., and Bean, B.P. (2015). Differential Regulation of Action Potential Shape and Burst-Frequency Firing by BK and Kv2 Channels in Substantia Nigra Dopaminergic Neurons. *J. Neurosci.* 35,

- 16404–16417. <https://doi.org/10.1523/JNEUROSCI.5291-14.2015>.
36. Miles, G.B., Dai, Y., and Brownstone, R.M. (2005). Mechanisms underlying the early phase of spike frequency adaptation in mouse spinal motoneurons. *J. Physiol.* 566, 519–532. <https://doi.org/10.1113/JPHYSIOL.2005.086033>.
37. Herrington, J., Zhou, Y.-P., Bugianesi, R.M., Dulski, P.M., Feng, Y., Warren, V.A., Smith, M.M., Kohler, M.G., Garsky, V.M., Sanchez, M., et al. (2006). Blockers of the Delayed-Rectifier Potassium Current in Pancreatic-Cells Enhance Glucose-dependent Insulin Secretion. *Diabetes* 55, 1034–1042.
38. Newkirk, G.S., Guan, D., Dombrow, N., Armstrong, W.E., Foehring, R.C., and Spain, W.J. (2022). Kv2.1 Potassium Channels Regulate Repetitive Burst Firing in Extratelencephalic Neocortical Pyramidal Neurons. *Cereb. Cortex* 32, 1055–1076. <https://doi.org/10.1093/CERCOR/BHAB266>.
39. Guan, D., Armstrong, W.E., and Foehring, R.C. (2013). Kv2 channels regulate firing rate in pyramidal neurons from rat sensorimotor cortex. *J. Physiol.* 591, 4807–4825. <https://doi.org/10.1113/JPHYSIOL.2013.257253>.
40. Bishop, H.I., Guan, D., Bocksteins, E., Parajuli, L.K., Murray, K.D., Cobb, M.M., Misonou, H., Zito, K., Foehring, R.C., and Trimmer, J.S. (2015). Distinct cell- and layer-specific expression patterns and independent regulation of kv2 channel subtypes in cortical pyramidal neurons. *J. Neurosci.* 35, 14922–14942. <https://doi.org/10.1523/JNEUROSCI.1897-15.2015>.
41. Guan, D., Tkatch, T., Surmeier, D.J., Armstrong, W.E., and Foehring, R.C. (2007). Kv2 subunits underlie slowly inactivating potassium current in rat neocortical pyramidal neurons. *J. Physiol.* 581, 941–960. <https://doi.org/10.1113/JPHYSIOL.2007.128454>.
42. Bortolami, A., Yu, W., Forzisi, E., Ercan, K., Kadakia, R., Murugan, M., Fedele, D., Estevez, I., Boison, D., Rasin, M.R., and Sesti, F. (2023). Integrin-KCNB1 potassium channel complexes regulate neocortical neuronal development and are implicated in epilepsy. *Cell Death Differ.* 30, 687–701. <https://doi.org/10.1038/s41418-022-01072-2>.
43. Altman, J., and Sudarshan, K. (1975). Postnatal development of locomotion in the laboratory rat. *Anim. Behav.* 23, 896–920. [https://doi.org/10.1016/0003-3472\(75\)90114-1](https://doi.org/10.1016/0003-3472(75)90114-1).
44. Nascimento, F., Spindler, L.R.B., and Miles, G.B. (2019). Balanced cholinergic modulation of spinal locomotor circuits via M2 and M3 muscarinic receptors. *Sci. Rep.* 9, 14051. <https://doi.org/10.1038/s41598-019-50452-1>.
45. Landoni, L.M., Myles, J.R., Wells, T.L., Mayer, W.P., and Akay, T. (2019). Cholinergic modulation of motor neurons through the C-boutons are necessary for the locomotor compensation for severe motor neuron loss during amyotrophic lateral sclerosis disease progression. *Behav. Brain Res.* 369, 111914. <https://doi.org/10.1016/j.bbr.2019.111914>.
46. Konsolaki, E., Koropouli, E., Tsape, E., Pothakos, K., and Zagoraiou, L. (2020). Genetic Inactivation of Cholinergic C Bouton Output Improves Motor Performance but not Survival in a Mouse Model of Amyotrophic Lateral Sclerosis. *Neuroscience* 450, 71–80. <https://doi.org/10.1016/j.neuroscience.2020.07.047>.
47. Smith, C.C., Brownstone, R.M., Bennet, L., and Farina, D. (2020). Spinal motoneuron firing properties mature from rostral to caudal during postnatal development of the mouse. *J. Physiol.* 598, 5467–5485. <https://doi.org/10.1113/JP280274>.
48. Smith, C.C., Paton, J.F.R., Chakrabarty, S., and Ichiyama, R.M. (2017). Descending Systems Direct Development of Key Spinal Motor Circuits. *J. Neurosci.* 37, 6372–6387. <https://doi.org/10.1523/JNEUROSCI.0149-17.2017>.
49. Kihira, Y., Hermanstynne, T.O., and Misonou, H. (2010). Formation of heteromeric Kv2 channels in mammalian brain neurons. *J. Biol. Chem.* 285, 15048–15055. <https://doi.org/10.1074/jbc.M109.074260>.
50. Stewart, R.G., Camacena, M., Copits, B.A., and Sack, J.T. (2024). Distinct cellular expression and subcellular localization of Kv2 voltage-gated K<sup>+</sup> channel subtypes in dorsal root ganglion neurons conserved between mice and humans. *J. Comp. Neurol.* 532, e25575. <https://doi.org/10.1002/cne.25575>.
51. Escoubas, P., Diochot, S., Célérier, M.L., Nakajima, T., and Lazdunski, M. (2002). Novel Tarantula Toxins for Subtypes of Voltage-Dependent Potassium Channels in the Kv2 and Kv4 Subfamilies. *Mol. Pharmacol.* 62, 48–57. <https://doi.org/10.1124/MOL.62.1.48>.
52. Ghezzi, F., Corsini, S., and Nistri, A. (2017). Electrophysiological characterization of the M-current in rat hypoglossal motoneurons. *Neuroscience* 340, 62–75. <https://doi.org/10.1016/J.NEUROSCIENCE.2016.10.048>.
53. Feinschreiber, L., Singer-Lahat, D., Friedrich, R., Matti, U., Sheinin, A., Yizhar, O., Nachman, R., Chikvashvili, D., Rettig, J., Ashery, U., and Lotan, I. (2010). Non-conducting function of the Kv2.1 channel enables it to recruit vesicles for release in neuroendocrine and nerve cells. *J. Cell Sci.* 123, 1940–1947. <https://doi.org/10.1242/JCS.063719>.
54. Deusch, E., Weigel, A.V., Akin, E.J., Fox, P., Hansen, G., Haberkorn, C.J., Loftus, R., Krapf, D., and Tamkun, M.M. (2012). Kv2.1 cell surface clusters are insertion platforms for ion channel delivery to the plasma membrane. *Mol. Biol. Cell* 23, 2917–2929. <https://doi.org/10.1091/MBE.E12-01-0047/ASSET/IMAGES/LARGE/2917FIG10.JPEG>.
55. Panzera, L.C., Johnson, B., Quinn, J.A., Cho, I.H., Tamkun, M.M., and Hoppa, M.B. (2022). Activity-dependent endoplasmic reticulum Ca<sup>2+</sup> uptake depends on Kv2.1-mediated endoplasmic reticulum/plasma membrane junctions to promote synaptic transmission. *Proc. Natl. Acad. Sci. USA* 119, e2117135119. <https://doi.org/10.1073/pnas.2117135119>.
56. Vierra, N.C., O'Dwyer, S.C., Matsumoto, C., Fernando Santana, L., and Trimmer, J.S. (2021). Regulation of neuronal excitation-transcription coupling by Kv2.1-induced clustering of somatic L-type Ca<sup>2+</sup> channels at ER-PM junctions. *Proc. Natl. Acad. Sci. USA* 118, e2110094118. <https://doi.org/10.1073/PNAS.2110094118>.
57. Kakizawa, S., Kishimoto, Y., Hashimoto, K., Miyazaki, T., Furutani, K., Shimizu, H., Fukaya, M., Nishi, M., Sakagami, H., Ikeda, A., et al. (2007). Junctophilin-mediated channel crosstalk essential for cerebellar synaptic plasticity. *EMBO J.* 26, 1924–1933. <https://doi.org/10.1038/SJ.EMBOJ.7601639>.
58. Harris-Warrick, R.M., Pecchi, E., Drouillas, B., Brocard, F., and Bos, R. (2024). Effect of size on expression of bistability in mouse spinal motoneurons. *J. Neurophysiol.* 131, 577–588. <https://doi.org/10.1152/JN.00320.2023/ASSET/IMAGES/MEDIUM/JN-00320-2023R01.PNG>.
59. Recabal-Beyer, A.J., Senecal, J.M.M., Senecal, J.E.M., Lynn, B.D., and Nagy, J.I. (2022). On the Organization of Connexin36 Expression in Electrically Coupled Cholinergic V0c Neurons (Partition Cells) in the Spinal Cord and Their C-terminal Innervation of Motoneurons. *Neuroscience* 485, 91–115. <https://doi.org/10.1016/j.neuroscience.2022.01.015>.
60. Dugué, G.P., Dumoulin, A., Triller, A., and Dieudonné, S. (2005). Target-Dependent Use of Coreleased Inhibitory Transmitters at Central Synapses. *J. Neurosci.* 25, 6490–6498. <https://doi.org/10.1523/JNEUROSCI.1500-05.2005>.
61. Bhumbra, G.S., and Beato, M. (2018). Recurrent excitation between motoneurons propagates across segments and is purely glutamatergic. *PLoS Biol.* 16, e2003586. <https://doi.org/10.1371/JOURNAL.PBIO.2003586>.
62. Lamotte d'Incamps, B., Bhumbra, G.S., Foster, J.D., Beato, M., and Ascher, P. (2017). Segregation of glutamatergic and cholinergic transmission at the mixed motoneuron Renshaw cell synapse. *Sci. Rep.* 7, 4037. <https://doi.org/10.1038/s41598-017-04266-8>.
63. Gray, M., and Santin, J.M. (2023). Series resistance errors in whole cell voltage clamp measured directly with dual patch-clamp recordings: not as bad as you think. *J. Neurophysiol.* 129, 1177–1190. [https://doi.org/10.1152/JN.00476.2022/ASSET/IMAGES/LARGE/JN.00476.2022\\_F008.JPEG](https://doi.org/10.1152/JN.00476.2022/ASSET/IMAGES/LARGE/JN.00476.2022_F008.JPEG).
64. Pearson, K.G., Acharya, H., and Fouad, K. (2005). A new electrode configuration for recording electromyographic activity in behaving mice. *J. Neurosci. Methods* 148, 36–42. <https://doi.org/10.1016/J.JNEUMETH.2005.04.006>.
65. Michel, M.C., Murphy, T.J., and Motulsky, H.J. (2020). New Author Guidelines for Displaying Data and Reporting Data Analysis and Statistical Methods in Experimental Biology. *J. Pharmacol. Exp. Ther.* 372, 136–147. <https://doi.org/10.1124/JPET.119.264143>.
66. Wasserstein, R.L., Schirm, A.L., and Lazar, N.A. (2019). Moving to a World Beyond “p < 0.05.”. *Am. Stat.* 73, 1–19. <https://doi.org/10.1080/00031305.2019.1583913>.
67. Makin, T.R., and De Vixry, J.J.O. (2019). Ten common statistical mistakes to watch out for when writing or reviewing a manuscript. *Elife* 8, e48175. <https://doi.org/10.7554/ELIFE.48175>.
68. Bernard, C. (2019). Changing the Way We Report, Interpret, and Discuss Our Results to Rebuild Trust in Our Research. *eNeuro* 6, ENEURO.0259-19.2019. <https://doi.org/10.1523/ENEURO.0259-19.2019>.
69. Ho, J., Tumkaya, T., Aryal, S., Choi, H., and Claridge-Chang, A. (2019). Moving beyond P values: data analysis with estimation graphics. *Nat. Methods* 16, 565–566. <https://doi.org/10.1038/s41592-019-0470-3>.

## STAR★METHODS

### KEY RESOURCES TABLE

REAGENT or RESOURCE	SOURCE	IDENTIFIER
<b>Antibodies</b>		
VACHT	Millipore	Cat#ABN100; RRID:AB_2630394
Alexa Fluor® 647 donkey anti-goat	Thermo Fisher Scientific	Cat# A-21447; AB_2535864
Alexa Fluor® 555 donkey anti-rabbit	Thermo Fisher Scientific	Cat# A-31570; RRID: AB_2563181
Alexa Fluor® 555 goat anti-mouse IgG1	Thermo Fisher Scientific	Cat# A-21127; RRID:AB_141596
mouse anti- KV2.2 IgG1	UC Davis/NIH NeuroMab Facility	K37/8; RRID:AB_2750662
rabbit anti- KV2.1	Millipore	Cat# AB5186-200UL; RRID:AB_2131651
goat anti-choline acetyltransferase	Millipore	Cat# AB144P; RRID:AB_2079751
Alexa Fluor® 488 donkey anti-goat	Thermo Fisher Scientific	Cat# A-11055; RRID: AB_2534102
3% normal donkey serum	Millipore	SC30-100ML
Triton X-100	Millipore	648464
<b>Chemicals, peptides, and recombinant proteins</b>		
GxTX-1E	Tocris	cat#5676
Muscarine	Sigma	cat#M6532
<b>Deposited data</b>		
<a href="https://github.com/Brownstone-lab/KV2_paper_Allfiles_for_jupyterNB">https://github.com/Brownstone-lab/KV2_paper_Allfiles_for_jupyterNB</a>	Github	N/A
<b>Experimental models: Organisms/strains</b>		
Hb9:eGFP mice; B6.Cg-Tg(Hlxb9-GFP)1Tmj/J	JAX	stock no. 005029
ChAT cre mice; B6; 129S6-Chatm2(cre)Lowl/J	JAX	stock no. 006410
KCNB1(+/-lox) mice	MRC Harwell	EMMA Strain ID: 08338
C57BL/6 mice	JAX	STRAIN CODE: 027
<b>Software and algorithms</b>		
FIJI image J	FIJI image J	RRID:SCR_002285
Microsoft Excel	Microsoft Corporation	RRID:SCR_016137
Anaconda package	Anaconda	RRID:SCR_018317
IMARIS	Bitplane	RRID:SCR_007370
Zen digital imaging	Zeiss	RRID:SCR_013672
<b>Other</b>		
Multiclamp 700A	Axon Instruments	RRID:SCR_021040
CED Power3 1401	CED Ltd	RRID:SCR_017282
P97 puller	Sutter Instruments	RRID:SCR_016842
Leica DMLFSA	Leica Microsystems	N/A
vibrating microtome Model 7000 smz-2	Campden Instruments Ltd	N/A
Vetbond	3M	No.1469SB
LSM 800 inverted confocal microscope	Zeiss	RRID:SCR_015963
Cryostat CM3050 S	Leica	RRID:SCR_016844
Grip strength test	Bioseb	N/A

### RESOURCE AVAILABILITY

#### Lead contact

Further information and requests for resources and reagents should be directed to and will be fulfilled by the [lead contact](#), Robert M. Brownstone ([r.brownstone@ucl.ac.uk](mailto:r.brownstone@ucl.ac.uk))

### Materials availability

No new materials were created for this work.

### Data and code availability

- Data: All data can be accessed from the following github repository: [https://github.com/Brownstone-lab/KV2\\_paper\\_Allfiles\\_for\\_jupyterNB](https://github.com/Brownstone-lab/KV2_paper_Allfiles_for_jupyterNB).
- Code: All code and Python analysis notebooks can be accessed from the following github repository: [https://github.com/Brownstone-lab/KV2\\_paper\\_Allfiles\\_for\\_jupyterNB](https://github.com/Brownstone-lab/KV2_paper_Allfiles_for_jupyterNB).
- Additional information: Any additional information required to reanalyse the data reported in this paper is available from the [lead contact](#) upon request.

## EXPERIMENTAL MODEL AND STUDY PARTICIPANTS

There are no human study participants.

### Animals

All experiments were approved by the University College London Animal Welfare and Ethical Review Body, and performed under Project Licences 70/9098 and PP2688499 granted under the Home Office Animals (Scientific Procedures) Act (1986).

Three different mouse lines were used for this work. Wild type C57BL/6J were acquired from Charles River Laboratories, Inc (strain code: 632) and used for breeding transgenic and conditional knockout (cKO) lines, and for patch clamp electrophysiology experiments targeting cortical pyramidal neurons. Heterozygous *Kcnb1*<sup>(+/lox)</sup> mice on a BL/6N background were acquired from the MRC Harwell facility (HA:006536; available through EMMA EM:08338), back-crossed to C57BL/6J mice, and bred to homozygosity (*Kcnb1*<sup>(lox/lox)</sup>). ChAT-IRES-Cre (ChAT<sup>(+/Cre)</sup>) mice were acquired from JAX (B6;129S6-Chatm2(cre)Low/J, stock no. 006410), and maintained on a C57BL/6J background. Hb9::eGFP mice, also maintained on a C57BL/6J background, were used for developmental immunohistochemistry (P2-21) and patch clamp experiments (P2-7). These mice were acquired from the Jessell lab in 2000 and are now available from JAX (B6.Cg-Tg(Hlxb9-GFP)1Tmj/J, stock no. 005029).

To generate *Kcnb1* cKO mice in which cholinergic neurons lack K<sub>v</sub>2.1 channels, *Kcnb1*<sup>(lox/lox)</sup> mice were crossed with ChAT<sup>(Cre/Cre)</sup> mice to produce ChAT<sup>(+/Cre)</sup>; *Kcnb1*<sup>(+/lox)</sup> offspring. Cre-positive animals with a floxed allele were then crossed back to *Kcnb1*<sup>(lox/lox)</sup> mice to produce ChAT<sup>(+/Cre)</sup>; *Kcnb1*<sup>(lox/lox)</sup> offspring (Figure 1).

The number and sex of animals used for each experiment are declared in the figure legends.

### Blinding and randomisation

For behavioural and anatomy experiments involving comparison of mature control and ChAT-K<sub>v</sub>2.1<sup>OFF</sup> mice, animals were assigned to groups based on their genotype and sex, but experimenters remained blinded to group identity throughout all experiments. For electrophysiology experiments, blinding was not possible before recording, so this was done before data analysis. For developmental anatomy experiments, experimenters were blinded after imaging had taken place due to obvious anatomical differences in tissue of different ages. Sections of all ages were stained simultaneously in batches and well order was randomised.

## METHOD DETAILS

### Immunohistochemistry

Animals were deeply anaesthetised by intraperitoneal injection of ketamine (100 mg kg<sup>-1</sup>) and xylazine (20 mg kg<sup>-1</sup>). Once insentient (loss of paw withdrawal), animals were perfused with 5 mL of phosphate buffered saline (PBS) followed by 20 mL of 4% paraformaldehyde. Vertebral columns were dissected and post-fixed for 24 h before spinal cords were dissected and cryoprotected in 30% sucrose for 72 h. Then, meninges were removed, and regions of interest segmented, frozen in OCT solution, and stored at -20°C. Transverse sections of 30–50 μm were cut using a cryostat (CM3050 S, Leica) and stored in 1x PBS as free floating sections.

To visualise motoneurons, C-boutons, and K<sub>v</sub>2.1 channels, sections were washed 3 times in PBS (10 min per wash) and then incubated for 1 h in blocking solution containing 3% normal donkey serum (NDS, SC30-100ML, Merk Millipore) and 0.2% Triton X-100 (648464, Merk Millipore) diluted in PBS (PBST). Sections were then incubated in blocking solution containing goat anti-choline acetyltransferase (ChAT, 1:250, Millipore Cat# AB144P; RRID:AB\_2079751) and rabbit anti- K<sub>v</sub>2.1 (1:500, Millipore Cat# AB5186-200UL; RRID:AB\_2131651) antibodies for 48 h at 4°C, then washed (3 × 10 min in 1xPBS) and incubated for 2 h at room temperature (22°C) in blocking solution containing the secondary antibodies Alexa Fluor 555 donkey anti-rabbit (1:500, Thermo Fisher Scientific Cat# A-31570, RRID: AB\_2563181) and Alexa Fluor 488 donkey anti-goat (Thermo Fisher Scientific Cat# A-11055; RRID: AB\_2534102, 1:500). Finally, sections were washed (3 × 10 min in 1xPBS) before being mounted on glass slides with Mowiol 4-88 (Carl Roth GmbH & Co. Kg).

To visualise C-boutons and K<sub>v</sub>2.2 channels, staining for goat anti-ChAT and mouse anti- K<sub>v</sub>2.2 IgG1 (UC Davis/NIH NeuroMab Facility, K37/89, RRID:AB\_2750662, 1:200) were done sequentially (ChAT first then K<sub>v</sub>2.2) using the same incubation times as above for each step. The same primary, secondary, and blocking solutions and concentrations were used for ChAT staining. For K<sub>v</sub>2.2 channels, NDS was

substituted for normal goat serum (NGS, 3%) and Alexa Fluor 555 goat anti-mouse IgG1 (Thermo Fisher Scientific Cat# A-21127; RRID:AB\_141596, 1:500) was the secondary antibody.

To determine whether the knockout strategy was successful, control (females, animals = 3, slices = 3 per animal, age = P21) and cKO (females, animals = 3, Slices = 3 per animal, age = P21) slices stained for ChAT and  $K_v2.1$  were imaged using a Zeiss LSM 800 confocal microscope (Zeiss LSM 800 inverted confocal microscope with Airyscan, RRID:SCR\_015963x), 20x objective (1 AU aperture) and Zeiss ZEN Blue Edition software (ZEN Digital Imaging for Light Microscopy, RRID:SCR\_013672). Tile scan images of spinal cord hemi-sections were stitched and opened in Image J analysis software (RRID:SCR\_002285) for processing. Using the particle analysis package, thresholding was performed on all images using the same settings to produce a black and white image showing only  $K_v2.1$  puncta. Regions of interest (ROI) of the same dimensions were defined to segment analyses of dorsal, intermediate, and ventral laminae. The nucleus counter function was then used to automatically produce a count of all puncta within the ROI, which was expressed as density (number per 100  $\mu\text{m}^2$ ).

### *Postnatal development of $K_v2.1$ and C-boutons on motoneurons*

Procedures for assessing the postnatal development of C-boutons and  $K_v2.1$  channels on lumbar motoneurons were largely the same as those described above, with a few differences. Lumbar (L4-5) sections were cut (50  $\mu\text{m}$ ) from neonatal (P2-3), transition (P6-7) and motor mature (P21) Hb9::eGFP transgenic mouse spinal cords. Vesicular Acetylcholine Transferase polyclonal antibody (VAChT, 1:500, Millipore Cat# ABN100; RRID:AB\_2630394) was used to visualize C-boutons and  $K_v2.1$  was visualised using the same antibody as described above. Secondary antibodies used were Alexa Fluor 647 donkey anti-goat (1:500, Thermo Fisher Scientific Cat# A-21447;AB\_2535864) and Alexa Fluor 555 donkey anti-rabbit (1:500, Thermo Fisher Scientific Cat# A-31570;RRID: AB\_2563181).

60x confocal z stack (0.4 $\mu\text{m}$  steps through tissue thickness) images were captured with the LSM 800 inverted confocal microscope and then pseudo-named in order to perform blinded analyses. Three-dimensional (3D) reconstructions of each motoneuron were then rendered using IMARIS Software (Bitplane, RRID:SCR\_007370) using the following procedure. First, in the 3D isometric view, solid surfaces of the motoneuron soma (Hb9::eGFP signal), C-boutons, and  $K_v2.1$  were created using the rendering and thresholding tools. The masking feature was then used to select  $K_v2.1$  clusters within 1  $\mu\text{m}$  of the motoneuron surface and VAChT<sup>+</sup> C-boutons. IMARIS was used to generate volume and surface area data for each motoneuron and associated C-boutons and  $K_v2.1$  clusters, and these were exported to an Excel (Microsoft Corporation, 2018, RRID:SCR\_016137) spreadsheet. Subsequent analyses were performed using python programming language run in Jupyter Labs environment. Cells were excluded only if quality of staining precluded accurate rendering of the cell.

Intensity plots were made in ImageJ by drawing a ROI with a polygon line around the perimeter of the cell, to connecting the centre points of all C-bouton puncta. The same ROI was copied to the  $K_v2.1$  channel and the relative intensities were measured (intensity/maximum intensity) for C-boutons and  $K_v2.1$ . The relative intensity values (y axis) were then plotted against the corresponding distance values (x axis).

## **Patch clamp electrophysiology**

### *Slice preparation*

Current clamp experiments were performed as described in Smith and Brownstone (2020). Mice of all ages were administered an intraperitoneal bolus of ketamine (100 mg kg<sup>-1</sup>) and xylazine (20 mg kg<sup>-1</sup>) and decapitated following loss of hind-paw withdrawal. The vertebral column was quickly excised and pinned (ventral-side-up) to a silicone dish containing ice-cold (0°C–4°C) normal artificial cerebrospinal fluid (nACSF) saturated with 95% carbogen. nACSF was made in 18 M $\Omega$  water with the following (in mM): 113 NaCl, 3 KCL, 25 NaHCO<sub>3</sub>, 1NaH<sub>2</sub>PO<sub>4</sub>, 2 CaCl<sub>2</sub>, 2 MgCl<sub>2</sub> and 11 D-glucose, pH 7.4 (Mitra & Brownstone, 2012). A vertebrectomy was performed to reveal the spinal cord, which was stripped of dura matter and extracted from the vertebral column. The spinal cord was then glued (3M Vetbond, No.1469SB) ventral-side-up to a pre-cut block of agarose (~8% in ddH<sub>2</sub>O) and mounted on a cutting chuck using superglue. These steps were completed as quickly as possible to ensure viability of slices from animals in the third post-natal week, typically within 3 min.

The chuck was transferred to the slicing chamber of a vibrating microtome (Model 7000 smz-2, Campden Instruments Ltd) containing ice-cold slicing solution made up of the following (in mM): 130 potassium gluconate, 15 KCL, 0.05 EGTA, 20 HEPES, 25 glucose, 3 kynurenic acid, pH 7.4.<sup>60,61</sup> 350  $\mu\text{m}$  slices were cut and transferred to the incubation chamber to rest in nACSF (32°C) for 30 min. The incubation chamber was then allowed to equilibrate to room temperature (maintained at 23°C) for at least 30 min before recording.

For voltage clamp experiments, animals were similarly anaesthetised and decapitated, and the spinal cord isolated, with oblique lumbar slices (350  $\mu\text{m}$  thick) made as previously described,<sup>62</sup> incubated at 37°C for 30–45min, and then maintained at room temperature (~20°C) prior to being used for experiments.

### *Recording and analyses: Current clamp*

Using a DMLFSA microscope (Leica DMLFSA; Leica Microsystems, Wetzlar, Germany), putative motoneurons were identified as the largest cells in the motor pools of the spinal cord. Patch pipettes were pulled using a P97 Flaming/Brown horizontal Micropipette Puller (Sutter Instrument, RRID:SCR\_016842) to a resistance of 1.5–4 M $\Omega$ . Patch pipette electrodes were filled with an internal solution consisting of (in mM): 131 K-methanesulfonate, 6 NaCl, 0.1 CaCl<sub>2</sub>, 1.1 EGTA, 10 HEPES, 0.3 MgCl<sub>2</sub>, 3 ATP-Mg, 0.5 GTP-Na, 2.5 L glutathionine, 5 phosphocreatine, pH 7.25 adjusted with KOH, osmolarity 290–300 mOsm.

Recordings were made using a MultiClamp 700A amplifier (Axon Instruments, Inc), low pass filtered at 10 kHz and digitized at 25 kHz using a CED Power3 1401 (Cambridge Electronic Designs Limited). All experiments were performed in current clamp mode and data captured

using Signal software (Cambridge Electronic Design Ltd, Cambridge, UK, RRID:SCR\_017282). Once whole cell configuration was achieved, the bridge was balanced, and capacitance neutralized prior to commencing recording. Motoneurons were injected with a small negative rectangular pulse (500 ms duration) and the voltage responses of 15–30 traces were averaged to measure input resistance and whole-cell capacitance (WCC). Resistance was measured as the peak voltage change to the injected current and  $\tau$  calculated from an exponential curve fitted to the response (automated in Signal). WCC was calculated using resistance and  $\tau$  values and cross-checked against the values automatically recorded by the software during the experiment. Rheobase was defined as the minimum amount of current needed to evoke an action potential. Motoneuron frequency-current ( $f$ - $I$ ) graphs were generated by injecting depolarizing current steps increasing from 0 nA until maximum firing was observed. The excitability of the cell (gain) was determined by measuring the slope of the main linear portion of  $f$ - $I$  plots for first interval frequency (instantaneous frequency of the first two spikes), and overall frequency (mean instantaneous frequency of all spike in a train). Action potential half widths (1/2 width), spike amplitude, and fast afterhyperpolarization (fAHP) were measured from 15 to 30 averaged single APs evoked with a 20 ms rectangular current pulse (to ensure stimulus artefact did not preclude measurement). The 1/2 width was calculated as the time between the 50% rise and 50% fall in amplitude of the AP. Spike height was measured as the voltage difference between the threshold (voltage at maximum positive value of the second derivative of membrane potential of AP) and the peak of the AP. The fAHP was measured as the difference between the voltage baseline and the most negative point on the first trough of the AP. Afterpotential measurements (mAHP amplitude and mAHP half decay time) were taken from averages of 15–30 single APs evoked with a 1 ms duration current pulse (to ensure stimulus artefact preceded mAHP). The mAHP amplitude was calculated from baseline to the most negative point on the trough. The mAHP half decay time is calculated as half the time taken (ms) from the most negative point of the mAHP to baseline. Cells were held at  $-65$  mV for single evoked APs.

### Recording and analysis: Voltage clamp

Motoneurons were visualized with a digital camera (Nikon, DS-Qi1Mc) using infrared differential interference contrast (DIC) optics on an Eclipse E600FN Nikon microscope (Nikon, Japan). Putative motoneurons were identified as above. For single electrode voltage-clamp recordings, a MultiClamp 700B or an Axopatch 200B amplifier (Molecular Devices, Sunnyvale) was used with signals filtered at 5 kHz and acquired at 50 kHz with a Digidata 1440A A/D board (Molecular Devices, Sunnyvale) and Clampex 10 software (Molecular Devices, Sunnyvale). A Flaming-Brown puller (P1000, Sutter Instruments, USA) was used to obtain borosilicate thick glass (GC150F, Harvard Apparatus, UK) pipettes, that were then microforged to a resistance of  $\sim 1$ – $3$  M $\Omega$  using a MF2 Narishige Microforge (Narishige Group, Japan). For dual electrode recordings, an additional electrode connected to a ELC-03X amplifier (NPI Electronics) was used in current clamp mode as a voltage follower. Patch pipettes were backfilled with an intracellular solution containing (in mM) 125 K-gluconate, 6 KCl, 10 HEPES, 0.1 EGTA, 2 Mg-ATP, pH 7.3 with KOH, and osmolarity of 290–310 mOsm.

To study outward currents, 500ms-long voltage steps from  $-90$  mV up to  $+110$  mV were applied in  $+10$  mV increments (2s-long sweeps), in the presence of CdCl<sub>2</sub> (100  $\mu$ M) and tetrodotoxin (TTX, 0.5  $\mu$ M) to reduce the effects of Ca<sup>2+</sup> and Na<sup>+</sup> channels activation. In some cases the amplitude of the largest step was adjusted accordingly to avoid damaging the cell, or the sweep length was increased to 5s or 10s. The current size was considered as the difference between the baseline and the amplitude of the last 20ms of the voltage step. To test the effect of GxTX-1E (100 nM), estimated currents were scaled to the maximum current amplitude obtained prior to toxin administration ( $I_{\max \text{ control}}$ ), and the largest values compared.

Series resistance, input resistance and holding voltage ( $V_{\text{hold}} = -90$  mV) were monitored throughout the experimental procedure in order to track the quality of the recordings before and after applying toxin. We employed a  $-5$  mV step prior to the positive voltage steps for studying K<sup>+</sup> currents, and from here the series resistance was calculated by dividing the voltage pulse by the amplitude of the observed transient peak current and input resistance by dividing the voltage step by the amplitude of the stable state current. The currents measured from lumbar motoneurons were several nA in amplitude, so we only included experiments in which the series resistance and input resistance did not differ more than  $\sim 25\%$  before and after application of GxTX-1E. Initial uncompensated series resistance was typically low ( $\sim 2$ – $6$  M $\Omega$ ), and compensation by 40%–80% was used to control variations before and after drug application; if the uncompensated series resistance changed  $>50\%$ , the recording was stopped to avoid unwanted voltage errors.<sup>63</sup> Inclusion and exclusion of voltage clamp experiments can be seen at [https://github.com/Brownstone-lab/KV2\\_paper\\_Allfiles\\_for\\_jupyterNB](https://github.com/Brownstone-lab/KV2_paper_Allfiles_for_jupyterNB).

For dual patch recordings, a second electrode attached to the same motoneuron monitored the real voltage of the cell, which was compared with the voltage command from the voltage clamp patch electrode and the predicted voltage estimated using the series resistance and Ohm's law as follows (2):

$$V_{\text{predicted}} = V_{\text{pipette}} - (R_{\text{series}} \times I_{\text{feedback}})$$

in which  $V_{\text{predicted}}$  is the calculated voltage estimate when taking into account the voltage error,  $V_{\text{pipette}}$  is the voltage command from the voltage clamp electrode,  $R_{\text{series}}$  is the series resistance and  $I_{\text{feedback}}$  is the measured current that flows across the amplifier's feedback resistor.

### Mature motoneurons

For these experiments, the experimental unit (N) was considered to be individual motoneurons and is disclosed in the results section and figure legend (as well as animal number and sex) for each experiment. To avoid sampling  $\gamma$ -motoneurons we selected the largest

motoneurons in motor pools with resting membrane properties consistent with those of verified  $\alpha$ -motoneurons- this was determined *a priori*. As a result, the majority of motoneurons sampled had input resistance values  $\leq 50$  M $\Omega$ . During analysis, we discovered a sampling bias between control and cKO motoneurons, whereby the control group had disproportionately more neurons with input resistance values  $>50$  M $\Omega$ . To account for this we only included motoneurons with input resistance values  $\leq 50$  M $\Omega$  (Figure 3B).

### Drugs and toxins

Baseline firing characteristics were recorded in nACSF for all experiments prior to the perfusion of drugs or toxins. To assess the effect of inhibiting  $K_V2$  channels, 100 nM GxTX-1E (Tocris, cat# 5676) in nACSF was perfused through the recording chamber for 10 min prior to the 2<sup>nd</sup> recording.<sup>20,34,38</sup> For experiments using muscarine (10 $\mu$ M, Sigma-Aldrich, cat# M6532), slices were perfused for 5 min prior to the 2<sup>nd</sup> recording.<sup>3,44,52</sup>

### Cortical pyramidal neuron patch clamp experiments

Coronal brain slices (350  $\mu$ m) were made from wild type C57BL/6J male mice aged P14-15 ( $N = 3$ ). Whole cell, current clamp recordings were made from visually identified pyramidal neurons in layer 5 of the cerebral cortex. Subsequent procedures were performed as described for mature motoneurons above.

### EMG recording for C-bouton motor amplification

Bipolar, intramuscular electrodes were fabricated using materials and methods described in detail by.<sup>64</sup>

Procedures for surgical implantation were also based on those first described by.<sup>64</sup> Mice were anaesthetised with isoflurane (5% with O<sub>2</sub>) and tested for loss of the paw withdrawal reflex before proceeding. Once insentient, the back and both hindlimbs were shaved, cleaned with 70% ethanol and then surgical iodine solution. An incision measuring the width of the EMG connector was made between the scapulae and another of similar size was made in the centre of the back at the level of the hips. Wires from the connector were tunnelled from the rostral to the caudal incision and the connector was secured in place using 4-0 sutures (ETHICON, W8683). Incisions were then made over the medial gastrocnemius and tibialis anterior of each hindlimb and corresponding wires tunnelled from the rostral incision to the muscle. Wires were inserted through the belly of the muscle up to the pre-made proximal knot in the wires and another distal knot was made to secure the recording sites in to muscle. The wires were trimmed, all incisions were washed with saline, and then closed with 7-0 sutures (ETHICON, W8702). Prior to withdrawing anaesthesia, the mouse was administered buprenorphine (Vetergesic, 0.1 mg/kg) and then transferred to a recover chamber maintained at 37°C until fully awake and ambulatory. Mice were given 1 drop of oral Metacam (Meloxicam, 1.5 mg/mL) analgesic daily for 5 days post-surgery, or as long as necessary.

After at least 10 full days of recovery, EMG recording sessions were undertaken. Immediately prior to recording, mice were lightly anaesthetised with isoflurane and the male connector was inserted into the female connector (sutured into the skin at the back of the neck). Once awake and ambulatory, mice were placed on a treadmill set to a speed of 0.15 m/s and recording commenced. Following walking experiments animals were transferred to a custom swimming pool (25°C) and muscle activity during swimming was recorded. Signals were amplified ( $\times 1000$ ) using an NL844 AC pre-amplifier (Digitimer Ltd) connected to an NL820 isolation amplifier (Digitimer Ltd), filtered (100 Hz-10KHz) and digitized with a Power 1401 interface and Spike2 software (Cambridge Electronic Design, Cambridge, United Kingdom).

### Behavioural assessments and analysis

#### Running wheel experiments

Experimental mice were housed in large (rat) cages (Allentown, NexGen Rat 900) separated into 2 compartments with a Perspex divider, perforated to allow some social interaction. One compartment housed a companion mouse, that had no access to a running wheel and the other was occupied by either a control (ChAT<sup>(w/w)</sup>;Kcnb1<sup>(f/f)</sup>) or KO mouse (ChAT<sup>(Cre/wt)</sup>;Kcnb1<sup>(f/f)</sup>) which had *ad libitum* access to an externally mounted running wheel (Panlab, LE905). Mice underwent an initial acclimation period (7 days) in which they had no access to the running wheel. Following acclimation, mice had 24 h access to the wheels and data were collected (Panlab multicounter, LE3806) in either 5 or 1 min epochs for a total of 16 h from 19:00 to 11:00. Running distances were calculated from the circumference of the wheels (50.24 cm) and the number of revolutions. Experiments lasted 5 weeks in males and 6 weeks in females, after which data were exported to Microsoft Excel spreadsheets and analyzed using Python scripts in the Jupyter notebooks environment. Animals were excluded only if determined to be non-compliant. Non-compliance was determined as the mouse running less than 500 m per 16 h period. Only 1 mouse was excluded for non-compliance.

#### Treadmill speed and endurance experiments

Mice were acclimatised to the treadmill (Panlab, multilane treadmill, LE8710MTS) for a period of 3 days before testing: On day 1, the belt was kept static and mice were allowed to explore for 10 min. On day 2, the treadmill was set to a 15% incline and mice walked slowly (5 cm/s) for a total time of 15 min. The air puff encouragement was activated when contact was made with a grid at the rear of the treadmill. Day 3 consisted of a 20 min session consisting of 2 min at 5 cm/s followed by increments of 2 cm/s every 2 min. On maximum speed testing days, mice were placed in the treadmill and the speed increased by 3 cm/s every minute for 5 min to warm up. Then, the speed was increased by 5 cm/s every 20 s until mice were persistently lagging (i.e., when total air puff stimulation reached 10s). After 2 days recovery, mice were subjected to

endurance tests involving the same 5 min warm up followed by up to 40 min (time cap) running at 60% of the maximum speed attained by individual mice. Again, the limit was determined as the time/distance at which mice received 10 s of air of stimulation.

### *Grip strength experiments*

Grip strength was tested using a grip strength meter (Bioseb, France; [Figure S5](#)) over 3 days, with 2 days rest between each session. The experimenter held the tail of the mouse whilst supporting its weight on their other hand before lowering it onto the horizontal metal grid attached to the grip strength meter. Once the mouse gripped the bars, the experimenter slowly pulled backwards by the tail until the mouse released its grip. The peak force (grams) was recorded and the mouse was returned to its cage to rest for 1 min. This process was repeated 3 times for each mouse on each day of testing. Thus, mean force outputs (normalised to weight g/g body weight) for each animal were calculated from a total of 9 'pulls'.

## QUANTIFICATION AND STATISTICAL ANALYSIS

We center our analyses on estimation statistics because it focusses conclusions on magnitude, precision and biological significance of the results, thereby circumventing many of the flaws associated with null hypothesis significance testing (NHST).<sup>65–68</sup> Hedges *g* effect sizes are calculated along with bootstrapped confidence intervals, which describe the range of effect sizes possible, rather than providing a single dichotomous decision (as done in NHST). Effect sizes can be classified as no effect (0–0.19), small (0.2–0.49), medium (0.5–0.79) and large (0.8; Hedges, 1981). Bootstrapped confidence intervals (CI) are used to determine the precision of the effect size; for confidence intervals that do not include 0, effect sizes are considered precise enough to attribute biological significance to the observed effects.

For unpaired comparisons of two groups, Gardner-Altman estimation plots were used, where the groups are plotted on the left axes and the Hedges *g* effect size with bootstrap resampled (5000 reshuffles) 95% confidence intervals plotted on the right. The Hedges *g* effect size is depicted as a dot; the 95% confidence interval is indicated by the vertical error bar. The values for mean difference ( $\mu$ ), effect size (*es*) and 95% confidence intervals [lower, upper] are displayed each plot. Experimental units (*N*) are described in the figure legends.

For paired experiments, Cumming paired estimation plots were used where the experimental units are plotted on the upper graphs and each paired set of observations is connected by a line. On the lower plots, effect sizes (Hedges *g*) are plotted with bootstrap resampled (5000 reshuffles) 95% confidence intervals. Effect sizes are depicted as dots; 95% confidence intervals are indicated by the vertical error bars. The bootstrapped mean differences ( $\mu$ ) are shown on the upper plots, and the effect sizes (*es*) and 95% confidence intervals [lower, upper] are displayed on the lower plots.

For IHC experiments assessing C-bouton and Kv2.1 channel expression and clustering during development, 3 animals (male) were used for each age group from which 3 sections and 16–18 motoneurons (maximum 6 per slice) were sampled. Because we were able to sample the entire motoneuron soma for puncta density measurements, we consider the motoneuron to be the experimental unit in these experiments.

For analysis of EMG data, signals acquired during walking and swimming were converted to RMS amplitudes ( $\tau = 40$  ms) and the peak values of each burst for each muscle were averaged. Motor amplification ratio was expressed as mean RMS amplitude during swimming/walking. Mean amplitudes across muscles (MG or TA) were treated as individual experimental units. For wheel running experiments assessing distance run per day, repeated measured ANOVAs were used as a suitable alternative was not available for estimation statistics.

All figures were created using Seaborn v.0.10.0, DABEST<sup>69</sup> and Matplotlib v.3.1.3 in the Python environment.